

# m6A is required for resolving progenitor identity during planarian stem cell differentiation

Yael Dagan<sup>1,†</sup>, Yarden Yescharim<sup>1,†</sup>, Ashley R Bonneau<sup>2,3,4</sup>, Tamar Frankovits<sup>1</sup>, Schraga Schwartz<sup>5</sup>, Peter W Reddien<sup>2,3,4</sup> & Omri Wurtzel<sup>1,6,\*</sup> 

## Abstract

Regeneration and tissue homeostasis require accurate production of missing cell lineages. Cell production is driven by changes to gene expression, which is shaped by multiple layers of regulation. Here, we find that the ubiquitous mRNA base-modification, m6A, is required for proper cell fate choice and cellular maturation in planarian stem cells (neoblasts). We mapped m6A-enriched regions in 7,600 planarian genes and found that perturbation of the m6A pathway resulted in progressive deterioration of tissues and death. Using single-cell RNA sequencing of >20,000 cells following perturbation of the m6A pathway, we identified an increase in expression of noncanonical histone variants, and that inhibition of the pathway resulted in accumulation of undifferentiated cells throughout the animal in an abnormal transcriptional state. Analysis of >1,000 planarian gene expression datasets revealed that the inhibition of the chromatin modifying complex NuRD had almost indistinguishable consequences, unraveling an unappreciated link between m6A and chromatin modifications. Our findings reveal that m6A is critical for planarian stem cell homeostasis and gene regulation in tissue maintenance and regeneration.

**Keywords** differentiation; m6A; planarian; regeneration; stem cells

**Subject Categories** Chromatin, Transcription & Genomics; Development

**DOI** 10.15252/embj.2021109895 | Received 6 October 2021 | Revised 10 July 2022 | Accepted 12 July 2022 | Published online 16 August 2022

**The EMBO Journal (2022) 41: e109895**

See also: [BW Benham-Pyle](#) (November 2022)

## Introduction

Tissue maintenance and regeneration depend on the production of the necessary cell types. At a tissue scale, cell signaling balances cell production and contributes to selection of cell fates. Yet, at the scale of an individual cell, it is the regulation of gene expression that

determines cell identity. Mechanisms that regulate gene expression of stem cells and other progenitors (e.g., dedifferentiated cells) are therefore central in the study of regeneration and tissue maintenance.

Recently, biochemical modifications to RNA molecules have emerged as regulators of gene expression. N6-methylation of adenosine (m6A) is a widespread modification to mRNAs, which is conserved from yeast to mammals. m6A modulates major aspects of RNA metabolism, including RNA stability, localization, and splicing (Yang *et al*, 2018). The mRNAs are decorated with methyl groups installed by a methyltransferase complex (MTC), composed of the methyltransferase METTL3 and accessory proteins, including METTL14, KIAA1429, WTAP, Hakai, RBM15/RBM15B, and ZC3H13 (Yang *et al*, 2018). The methylated sites are recognized by several reader proteins including YTH-domain containing proteins affecting gene expression (Patil *et al*, 2018). Studies in multiple organisms have shown that m6A and many components of the m6A pathway are essential for diverse processes: meiosis in the yeast *Saccharomyces cerevisiae* (Schwartz *et al*, 2013), oogenesis and sex determination in *Drosophila melanogaster* (Hongay & Orr-Weaver, 2011; Kan *et al*, 2017), early development in mammals (Geula *et al*, 2015), B-cell development (Zheng *et al*, 2020), and hematopoiesis (Zhang *et al*, 2017). m6A is therefore a key regulator of dynamic processes involving cellular proliferation and differentiation, and thus it could play an important role in tissue regeneration.

Planarians are flatworms that can regrow and support any adult tissue using a heterogeneous population of stem cells known as neoblasts (Rink, 2013). Following injury, neoblasts rapidly divide and grow a blastema that forms missing tissues. During homeostasis, neoblasts support existing tissues by continuously replacing them. The plasticity of individual neoblasts requires stringent regulation of gene expression (Wagner *et al*, 2012; Rink, 2013; Adler & Sánchez Alvarado, 2015). Consequently, neoblast gene expression determines lineage selection (van Wolfswinkel *et al*, 2014; Molinaro & Pearson, 2018), cell cycle progression (Raz *et al*, 2021), and cellular migration (Sahu *et al*, 2021). Transcriptional regulation has been studied at multiple resolutions in planarians: extracellular signaling

<sup>1</sup> The George S. Wise Faculty of Life Sciences, School of Neurobiology, Biochemistry, and Biophysics, Tel Aviv University, Tel Aviv, Israel

<sup>2</sup> Whitehead Institute for Biomedical Research, Cambridge, MA, USA

<sup>3</sup> Department of Biology, Massachusetts Institute of Technology, Cambridge, MA, USA

<sup>4</sup> Howard Hughes Medical Institute, Chevy Chase, MD, USA

<sup>5</sup> Department of Molecular Genetics, Weizmann Institute of Science, Rehovot, Israel

<sup>6</sup> Sagol School of Neuroscience, Tel Aviv University, Tel Aviv, Israel

\*Corresponding author. Tel: +972 3 6409553; E-mail: owurtzel@tauex.tau.ac.il

<sup>†</sup>These authors contributed equally to this work

and other systemic signals that regulate neoblast biology have been studied in depth over the past decade. Epigenetic regulators that modify the chromatin landscape and alter fate determination were discovered (Duncan *et al*, 2015). Transcription factor expression that is associated with differentiation to distinct planarian lineages has been described (van Wolfswinkel *et al*, 2014). However, molecular and functional studies of mRNA methylation have not been reported in planarians, and their impact on tissue homeostasis and regeneration is unknown.

Here, we analyzed the functions of planarian genes encoding components of the m6A-modification pathway (m6A genes) and studied the consequence of their inhibition. We mapped m6A-enriched regions in 7,600 genes expressed in a diversity of cell types and conditions. We identified multiple roles for the m6A pathway in neoblast biology, including regulation of cell fate choice, cell cycle control, and production of polyadenylated histone variants. Inhibition of m6A genes resulted in coordinated overexpression of adjacent genes in repetitive genomic regions, which were transcriptionally silenced in control animals. Systematic reanalysis of >1,000 planarian gene expression datasets revealed striking molecular similarities following silencing of the nucleosome remodeling and deacetylase complex (NuRD) component *CHD4*, suggesting a functional association between m6A and chromatin regulation. Single-cell RNA sequencing (scRNAseq) and confocal imaging revealed an accumulation of a previously undescribed class of cells following inhibition of m6A genes and of NuRD. Our study reveals that m6A is ubiquitous in planarians, establishes assays for studying m6A on a genomic scale, and reveals critical functions of m6A genes that are fundamental to regeneration and homeostasis.

## Results

### Components of m6A pathway are broadly expressed in planarians

We identified planarian genes that encode putative components of the MTC by searching for genes in the planarian genome encoding proteins similar to known MTC components in human, yeast, and fruit fly (Materials and Methods). We detected sequences corresponding to all of the canonical MTC components (Figs 1A and EV1A; Appendix Tables S1 and S2). We identified six putative genes encoding m6A readers in the planarian genome by searching the YTH-domain signature in the predicted planarian proteome (Figs 1A and EV1B). Orthologs of these putative YTH-encoding genes were found in six additional planarian species (Materials and Methods). By comparison, *Drosophila melanogaster* has two YTH-containing genes and vertebrates have five genes encoding a YTH-domain (Lence *et al*, 2017), suggesting that the YTH gene family is expanded in planarians.

We analyzed the expression of the genes that encode m6A-pathway components (m6A genes) across cell types in the planarian cell lineage atlas (Plass *et al*, 2018). We found that m6A genes are expressed across multiple cell types and particularly in neoblasts (Fig EV1C and D). Genes that encode YTH-domain were expressed in largely nonoverlapping cell types, suggesting that these putative readers might have distinct functions, which are activated in a cell-type-specific manner (Fig EV1D). Only one YTH-domain gene, *ythdc-1*, was expressed broadly and across cells in multiple stages of differentiation. Analysis

of MTC gene expression showed that MTC-encoding genes were expressed during the differentiation of multiple lineages and in multiple cell types (Fig EV1C). This suggests that m6A has a role in cellular differentiation in planarians, and that it might modulate different aspects of RNA metabolism using distinct m6A readers.

### m6A pathway activity is required for planarian regeneration and homeostasis

We studied the function of the m6A pathway in planarians by systematically inhibiting the m6A genes using RNAi (Materials and Methods). Inhibition of components of the MTC encoded by *kiaa1429* and *mettl14* resulted in a smaller body size compared with control animals, failure to uptake food, and eventually in lysis (Figs 1B and EV1E–G). Inhibition of other MTC-encoding genes did not result in a penetrant phenotype, yet inefficient inhibition of gene expression could explain this result (Batista *et al*, 2014; e.g., of *mettl3*; Fig EV1H). Inhibition of the predicted m6A reader, *ythdc-1*, resulted in a similar phenotype (Figs 1B and EV1G). Interestingly, *ythdc-1* is the only m6A reader gene that is broadly expressed across cell types and stages of lineage differentiation (Fig EV1D). Next, we tested the ability of animals to regenerate following inhibition of the m6A pathway by feeding the animals with dsRNA and amputating them. Inhibition of both MTC-encoding genes and *ythdc-1* eliminated the ability of the animals to regenerate. For example, amputated *kiaa1429* (RNAi) animals did not produce a blastema and consequently died (Fig 1B). We tested if this rapid effect was an outcome of depletion of m6A or a nonspecific off-target effect of the RNAi. We tested the specificity of the *kiaa1429* (RNAi) phenotype by repeating the experiment using a nonoverlapping dsRNA construct and found comparable phenotypes (Fig EV1I and J; Materials and Methods). Next, we quantified the m6A levels of RNA from *kiaa1429* (RNAi), *mettl14* (RNAi), and control animals using an anti-m6A-antibody (Materials and Methods). We detected 3.3- and 2.2-fold reduction (Student's *t*-test  $P < 0.05$ ) in the level of m6A (Fig 1C) following inhibition of *kiaa1429* and *mettl14*, respectively. Next, we tested if m6A was found on planarian mRNA or on functional non-polyadenylated transcripts. Polyadenylated RNA was over fourfold enriched with m6A (Fig 1D;  $P < 0.05$ ). These results demonstrate that (i) planarian m6A genes are required for regeneration and tissue homeostasis, (ii) that the MTC genes are required for installing m6A, and (iii) that m6A is enriched on mRNA.

### m6A is abundant on planarian mRNAs

We next mapped m6A-enriched regions in planarian RNAs by using m6A-seq2 (Dierks *et al*, 2021). m6A-seq2 allows multiplexed antibody-based m6A profiling of multiple samples in a single tube, thereby also permitting quantitative comparison of methylation levels across diverse samples (Fig 2A; Materials and Methods; Appendix Table S3). RNA was extracted from control animals, having normal m6A levels, and from *kiaa1429* (RNAi) animals, having depleted m6A (Figs 1C and 2A). m6A-seq2 confirmed that mRNA originating from *kiaa1429* (RNAi) animals was enriched substantially and significantly less than the control counterparts (Fig EV2A), and that far fewer “peaks,” and of decreased intensity, were detected in the *kiaa1429* (RNAi) animals in comparison to the controls (Fig EV2A–D; Materials and Methods). We mapped the

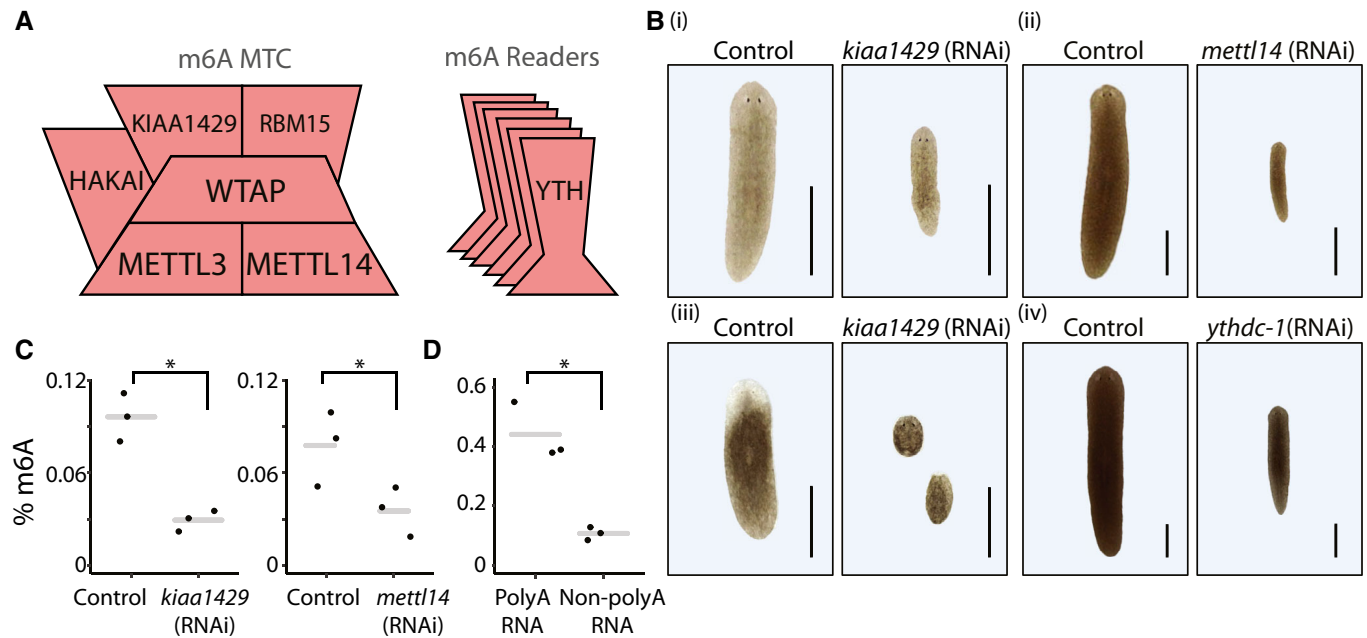


**Figure 1. Expression of m6A genes is required for planarian regeneration and viability.**

**A** Components of the m6A MTC (left) and readers (right) that were identified in the planarian genome (Fig EV1A and B; Materials and Methods).  
**B** Effect of RNAi on planarian homeostasis and regeneration. Gene expression was inhibited by feeding the animals with dsRNA against the target gene (Materials and Methods). Phenotypes were observed in *kiaa1429* (RNAi) animals following five dsRNA feedings in homeostasis (i); 10/10 animals), in regeneration (ii); 10/10 animals; shown 10 days post amputation), and following nine feedings of *mettl14* (iii) or *ythdc-1* dsRNA feedings (iv). Matching controls did not show phenotypes ( $n = 10$  per control group). Experiments were performed at least three times with over 10 animals per experiment in each experimental group. Scale = 1 mm.  
**C, D** The relative abundance of m6A was estimated by using an anti-m6A-antibody (Materials and Methods), showing similar m6A levels compared to recent quantification of m6A in mammals (Liu et al, 2020b); (C) Quantification of m6A on RNA isolated from *kiaa1429* (RNAi) and control animals following five RNAi feedings (left), or from *mettl14* (RNAi) and control animals following nine RNAi feedings (right), revealed a strong reduction in m6A levels following inhibition of gene expression (Student's *t*-test  $P < 0.05$ ). (D) Comparison of m6A levels on polyadenylated and non-polyadenylated RNA showed that polyadenylated RNA was highly enriched in m6A (Student's *t*-test  $*P < 0.05$ ).

sequencing data to the planarian genome and detected regions enriched following IP in comparison to input ("m6A peaks") via MeTPeak (Cui et al, 2016; Fig 2A and B; Materials and Methods). The read mapping was similar across all libraries (84–90%, SD = 1.5%; Appendix Table S4), without a significant difference between the mapping of m6A-enriched libraries and their input controls and between *kiaa1429* (RNAi) and their controls (Materials and Methods). Reads were aligned to >20 k genes, producing a comprehensive map of the planarian m6A transcriptome (Dataset EV1). We detected 7,600 genes having m6A peaks enriched by >5-fold over input in the control m6A libraries (MeTPeak score <1E-4). Many peaks were detectable following inhibition of *kiaa1429*, but their enrichment score was significantly reduced (Figs 2B and EV2B–D; Dataset EV1;  $P = 2.5E-6$ ). We divided the genes to bins based on their expression in the input libraries and examined m6A-enriched regions in each bin. The most highly expressed genes (bin 10) had fewer m6A peaks compared with genes in bins 6–9 (Fig 2C), an observation consistent with findings in mammalian systems (Dominiissini et al, 2012; Schwartz et al, 2014). Interestingly, m6A was not detected on rRNA (Fig EV2E), in contrast to mammalian systems where two sites are installed via a mechanism independent of METTL3, which could contribute to the lower m6A detection in non-polyA RNA (Fig 1D). m6A peaks were strongly biased toward the 3' end of transcripts, similar to the case in mammalian systems,

a trend that was not observed in the input samples (Fig 2B). Interestingly, the peak length distribution in planarians was longer than observed in other organisms (Liu et al, 2020c; Fig 2D). We validated this result by mixing planarian and yeast (*S. cerevisiae* sk1) RNA and processing the mixed sample according to the m6A-seq2 protocol (Fig EV3, Dataset EV1; Materials and Methods). The mixed RNA sample processing included RNA fragmentation, 3'-end barcoding, m6A enrichment, library preparation, and sequencing, therefore reducing many of the technical aspects that could contribute to the increased fragment length observed in planarian m6A peaks. We mapped the sequenced mixed libraries to the planarian and yeast genome and performed m6A peak detection (Fig EV3A–E; Materials and Methods). Yeast m6A peak lengths (median = 198 nt, s.d. = 222) were similar to those previously published in the REPIC database (Liu et al, 2020c; Fig EV3B) and were significantly shorter compared with planarian m6A peaks detected in this experiment (median 298 nt, s.d. = 222; Student's *t*-test = 2.2E-16). The distribution of planarian m6A peaks was similar to our initial mapping experiment (Fig EV3C) and longer than observed in other organisms.

The increased length of planarian m6A peaks rendered the detection of the m6A installment motif DRACH (D = A/G/U; R = A/G; H = A/C/U) (Linder et al, 2015) challenging. We therefore used high-confidence m6A-enriched regions shorter than 250 bp (Fig EV3D–G; Materials and Methods; top 500 enriched peaks).

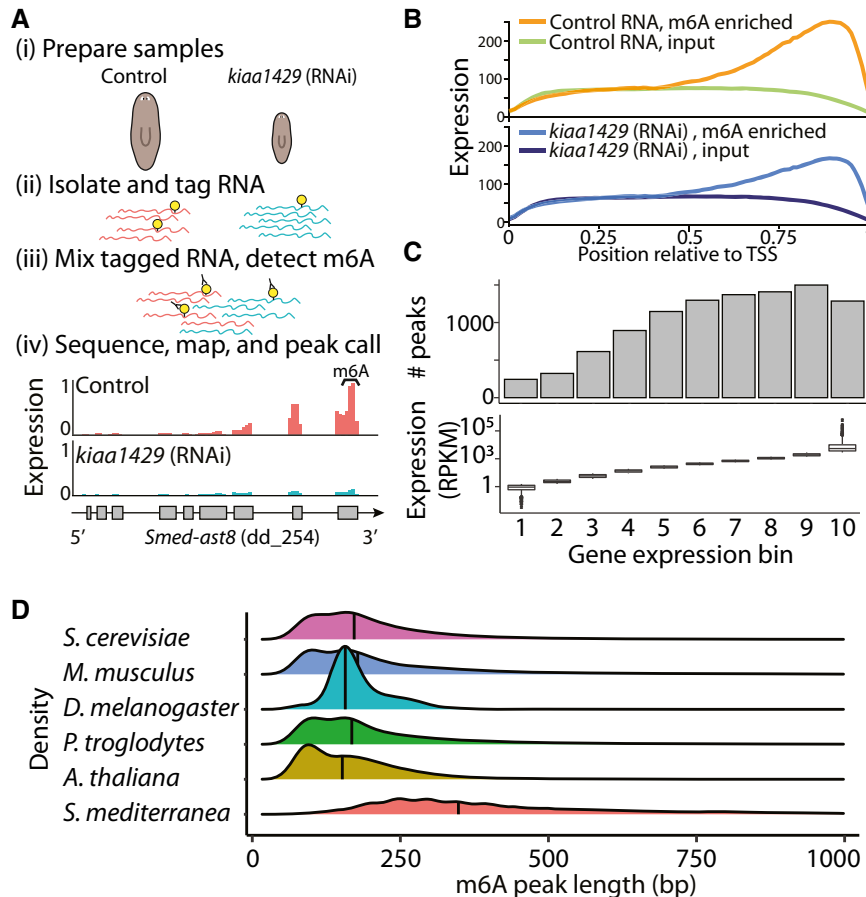


**Figure 2. Transcriptome-wide mapping of m6A in planarians.**

- A** Outline of mapping of m6A on planarian RNA. RNA was extracted from control or *kiao1429* (RNAi) animals in triplicates, with at least 10 animals in each replicate (i). Then, RNA was molecularly tagged with a barcoded RNA oligo (ii). Samples of barcoded RNA were mixed, and methylated RNA was enriched using an anti-m6A-antibody; input samples were sequenced without anti-m6A-antibody enrichment (iii). RNA was used for RNAseq library preparation, and resultant libraries were sequenced. Sequencing data was mapped to the planarian genome, and m6A-enriched regions (peaks) were detected using MeTPeak (Cui et al, 2016); read coverage across *Smed-ast8* is shown as normalized RPKM that was scaled to 0–1 across samples (iv).
- B** m6A peaks are highly enriched at the 3' end of the transcript. X-axis shows the relative position to the transcription start site (TSS); transcript lengths were normalized to 1,000 nt. Y-axis is the average peak expression (normalized by RPKM) across 740 high-confidence peaks ( $\geq 10$  fold-enriched). Plot produced using the deepTool-s2 package (Ramírez et al, 2016) (Materials and Methods).
- C** The number of m6A peaks, which were determined using MeTPeak (Cui et al, 2016), is shown (top) as a function of gene expression in each bin (bottom, box plot).
- D** The distribution of the m6A peak length as detected by MeTPeak; peak length was limited to up to 1,000 nt for visualization. Black line represents the median peak length. Processed data for organisms other than planarian were obtained from REPIC (Liu et al, 2020c).

Using this approach, CGACC, which is similar to the DRACH motif, was found to be the most enriched sequence. These results were recapitulated on the basis of a separate analysis pipeline (Schwartz et al, 2014; Dierks et al, 2021), which we applied to both yeast and planarian data. This analysis also revealed an enrichment for “GAC” harboring motifs in planarians and the GGACA motif in yeast (Fig EV3F and G). Thus, m6A maps in planarians exhibit many of the classical hallmarks of m6A: they are enriched toward the ends of genes, depleted from highly expressed genes, are enriched in a “GAC” motif, and are highly depleted upon inhibition of *kiao1429*. The increased length of planarian m6A-enriched regions may suggest that planarian m6A sites are found in spatial proximity in RNA molecules, and higher-resolution mapping of m6A sites could be used to further test this hypothesis.

### m6A genes regulate neoblast gene expression

The animal size reduction and lysis following inhibition of expression of m6A genes suggested that the animals were unable to produce cells normally. Failure to maintain and generate tissue is often a consequence of neoblast depletion or failure of neoblasts to differentiate (Reddien et al, 2005; Lin & Pearson, 2014; Zhu et al, 2015). We tested whether neoblasts were depleted following m6A-pathway inhibition by counting neoblasts by fluorescent *in situ* hybridization (FISH; Materials and Methods) using two canonical neoblast markers, *smedwi-1* (Reddien et al, 2005) and *h2b* (Guo et al, 2006). The number of *smedwi-1*<sup>+</sup> or *h2b*<sup>+</sup> cells per unit area was similar following inhibition of *kiao1429* gene expression (Fig 3A and B). Therefore, the phenotypes were not a consequence of neoblast depletion.

Our FISH approach allowed counting neoblasts using neoblast markers, but not to measure gene expression levels. We used quantitative reverse transcription PCR (qPCR) for measuring *smewi-1* and *h2b* expression level following RNAi on polyadenylated RNA (Fig 3C and D; Materials and Methods). We saw no significant change in *smewi-1* gene expression in all of the tested RNAi conditions. By contrast, we found a significant upregulation of up-to 14-fold in *h2b* expression following inhibition of m6A genes. *h2b* was overexpressed even in conditions that did not produce a lysis phenotype (Fig 3D). The overexpression of *h2b* suggested that changes to neoblast gene expression preceded the development of the RNAi phenotype.

Expression of *h2b* is a hallmark of neoblast cell-cycle progression (Guo et al, 2006; Wenemoser & Reddien, 2010; Solana et al, 2012). We therefore tested whether the expression of m6A genes was required for normal cell cycle regulation. The relative abundance of cell cycle states was analyzed by fluorescence-activated cell sorting (FACS) of Hoechst-labeled planarian cells from control and *kiaa1429* (RNAi) animals (Fig 3E and F; Materials and Methods). G1 neoblasts and recently divided post-mitotic progenitors are found specifically in a FACS gate called X2 (Hayashi et al, 2006). Our FACS analysis (Fig 3E and F) revealed a sixfold increase in the number of cells in the X2 gate following *kiaa1429* RNAi and more minor changes in the number of cells in the G2/M gate (X1) or in fully differentiated cells (Xins). The increase in the X2 cell population could be a consequence of an increase (i) in G1 neoblasts; (ii) in post-mitotic progenitors; or (iii) in both. We considered these options. The FACS analysis revealed that there was a minor change in the abundance of S-phase and G2 cells (Fig 3E and F). In addition, FISH revealed that there was no absolute change in neoblast number following *kiaa1429* (RNAi), as determined by *smewi-1*<sup>+</sup> or *h2b*<sup>+</sup> cell labeling (Fig 3A). Taken together, these data suggested that the population size of G1/S/G2 neoblasts did not change dramatically. We further tested this hypothesis using two approaches. First, we used an anti-H3P antibody to label mitotic cells and counted H3P+ cells found in a defined region anterior to the pharynx (Fig EV4A and B; Materials and Methods). We found no significant increase ( $P = 0.59$ ) in the number of H3P+ cells following inhibition of *kiaa1429*, which indicated that the neoblast population mitotic rate is unperturbed. In addition, we estimated the number of cells going through S-phase in *kiaa1429* (RNAi) and control animals by metabolic labeling using the thymidine analog, F-ara-EdU. Animals were soaked in F-ara-EdU for 16 h and were then immediately fixed for further processing. Following F-ara-EdU detection, the F-ara-EdU+ cells were counted in a ventral sub-epidermal layer that is distinguishable from the intestine (Fig EV4C and D; Materials and Methods). We found no significant difference in the number F-ara-EdU+ cells between the *kiaa1429* (RNAi) and control animals, which further indicated that in the conditions tested here, there was no detectable defect in neoblast cell cycle progression. Therefore, the increase in X2 cell abundance was most likely a consequence of an increase in the number of immature *smewi-1*<sup>-</sup> post-mitotic progenitors, and not of G1 neoblasts, which are *smewi-1*<sup>+</sup>.

#### m6A genes regulate cell-type-specific gene expression programs

The increase in post-mitotic progenitors following the inhibition of m6A pathway components may have affected multiple cellular

lineages and gene expression programs. We profiled the emergence of gene expression changes following inhibition of *mettl14* and *ythdc-1* after four, six, and eight RNAi feedings (Fig 4A; Dataset EV2; Materials and Methods). The phenotype of *kiaa1429* (RNAi) animals developed more rapidly, and therefore, we measured gene expression changes only following five RNAi feedings (Fig 4B). The gene expression changes following *mettl14* (RNAi) and *ythdc-1* (RNAi) were remarkably similar, with correlation >0.7 between all time points (Fig 4A–C). Comparison of *mettl14* (RNAi) or *ythdc-1* (RNAi) with *kiaa1429* (RNAi) resulted in high correlation as well, 0.56 and 0.46, with *mettl14* (RNAi) or *ythdc-1* (RNAi), respectively (Appendix Fig S1A and B), despite the time point differences associated with the rapid development of the *kiaa1429* (RNAi) phenotype. The sequencing validated the specificity of our RNAi and corroborated our qPCR results (Fig 4A and B; Appendix Fig S1C–F). This indicated that the phenotypes were a consequence of m6A depletion and not m6A-independent functions of the MTC.

The presence of m6A has been previously associated with a high transcript turnover rate (Lee et al, 2020; Zaccara & Jaffrey, 2020). Therefore, we predicted that inhibition of the m6A pathway would result in an overexpression of transcripts at early stages of the phenotype emergence. Indeed, following four RNAi feedings, most differentially expressed genes were upregulated: 77 and 83% for *mettl14* (RNAi) and *ythdc-1* (RNAi), respectively (Appendix Fig S1G; Dataset EV2). By contrast, at late time points, most differentially expressed genes were downregulated (Appendix Fig S1G), which likely reflected the indirect effects of m6A gene inhibition, such as depletion of a cell type.

We annotated differentially expressed genes using the planarian cell-type transcriptome atlas (Fincher et al, 2018). The majority of the upregulated genes following RNAi were not cell-type-specific (Dataset EV2), nor did they share a common function (Rozanski et al, 2019) or have association with the injury response (Wurtzel et al, 2015). By contrast, a major fraction of the downregulated genes were cell-type specific and were normally expressed in the planarian intestine and intestine-associated neoblasts (Fincher et al, 2018; Plass et al, 2018; Fig 4A, B and D). For example, the transcription factor *nkx-2.2*, which is required for specification of intestine cells (Forsthoefel et al, 2012), was downregulated following RNAi, and similarly, *activin-1* expression was reduced. The reduction in intestine-specific gene expression was observed already following four RNAi feedings, but it was exacerbated at later time points (Fig 4A and B; Dataset EV2).

To test whether the reduction in intestinal gene expression represented downregulation of a gene expression program or a reduction in intestine cell number, we analyzed by FISH *kiaa1429* (RNAi), *mettl14* (RNAi), and *ythdc-1* (RNAi) and control animals using a riboprobe labeling the planarian intestine (Figs 4E and EV4E–G). We found a severe defect in intestinal branching morphology following *kiaa1429* (RNAi) (Figs 4E and EV4F, Materials and Methods), which suggested that the RNAi resulted in depletion of intestine cells. Indeed, following inhibition of *kiaa1429*, animals did not uptake food (Fig EV1F). Inhibition of *mettl14* (RNAi) and *ythdc-1* (RNAi) resulted in a significant decrease of 43% and 57% in the number intestinal cells, respectively, without loss of intestine morphology (Fig EV4E–G) at the time point tested (Bonferroni corrected

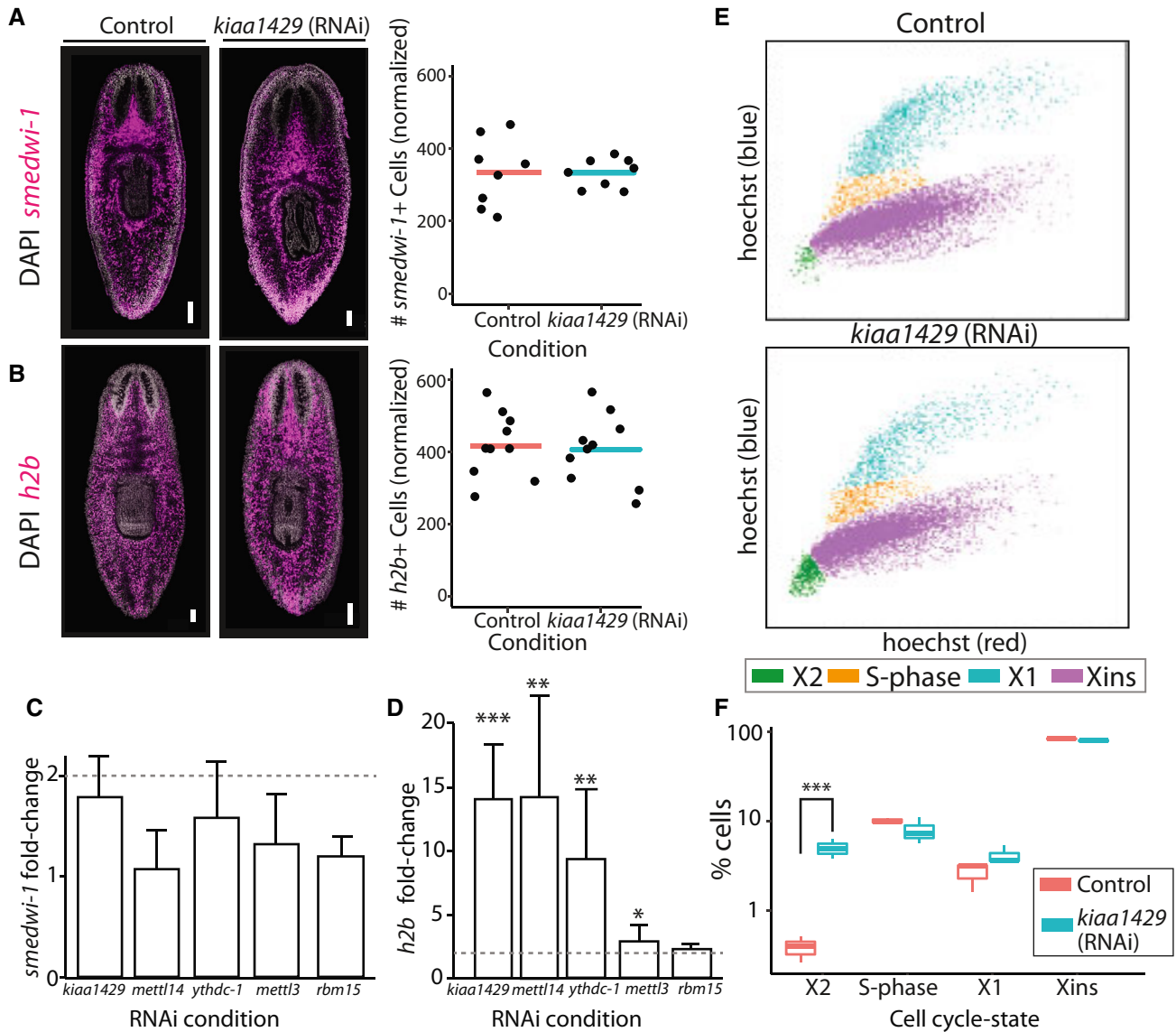


**Figure 3. m6A pathway expression is not required for neoblast viability.**

**A, B** The number of neoblasts did not change significantly following inhibition of the MTC-gene *kiaa1429*. Shown is FISH of *smedwi-1* (A) and *h2b* (B) in control and *kiaa1429* (RNAi) animals (left). *smedwi-1*<sup>+</sup> or *h2b*<sup>+</sup> cells were counted following FISH and showed no significant difference in expression (right; bar represents average normalized cell count; [Materials and Methods](#)). Scale = 100 μm.

**C, D** Gene expression analysis of *smedwi-1* (C) and *h2b* (D). The expression of *smedwi-1* and *h2b* was determined in the different RNAi conditions compared to the expression of these genes in control animals ([Materials and Methods](#)). Dashed line marks a twofold change in expression. Measurements performed on biological triplicates. *P*-value was calculated by two-sided Student's *t*-test followed by Bonferroni correction for multiple hypotheses. Lack of asterisk indicated a non-significant change in gene expression. Error bars indicate the 95% confidence interval (\*\*\**P* < 0.001, \*\**P* < 0.01, \**P* < 0.05).

**E** Representative FACS plots of cells isolated from control (top) and *kiaa1429* (RNAi) animals (bottom) show an increase in cell abundance in the X2 gate (green; [Materials and Methods](#)).

**F** Quantification of the cells in each FACS gate in control and *kiaa1429* (RNAi) animals showed a sixfold increase in the abundance of cells in the X2 gate (Student's *t*-test \*\*\**P* < 0.005). FACS experiments were performed in biological triplicates. Boxes represent the IQR, whiskers represent the 1.5 × IQR, and central band represents the median.

Student's *t*-test *P* < 0.05 for both conditions). This result was consistent with the observation that inhibition of *kiaa1429* resulted in a more rapidly developing phenotype. To test whether there was a major depletion in other cell types, we performed FISH using five other cell type markers for muscle,

neuron, epidermal lineage, *cathepsin* + cells, and protonephridia on *kiaa1429* (RNAi) animals (Fig 4E). The general defect in *kiaa1429* (RNAi) body morphology (Fig 1B) limited the ability to quantify the abundance of individual cell types. Yet, cell-type-specific FISH labeling demonstrated that all major cell types

were distributed across the animal, with the exception of intestine cells (Fig 4E). Importantly, cell types and lineages other than the intestine might have been affected by the RNAi, yet

other factors, such as the cell-type-specific turnover rate, might have caused the intestine to develop a significant defect more rapidly.

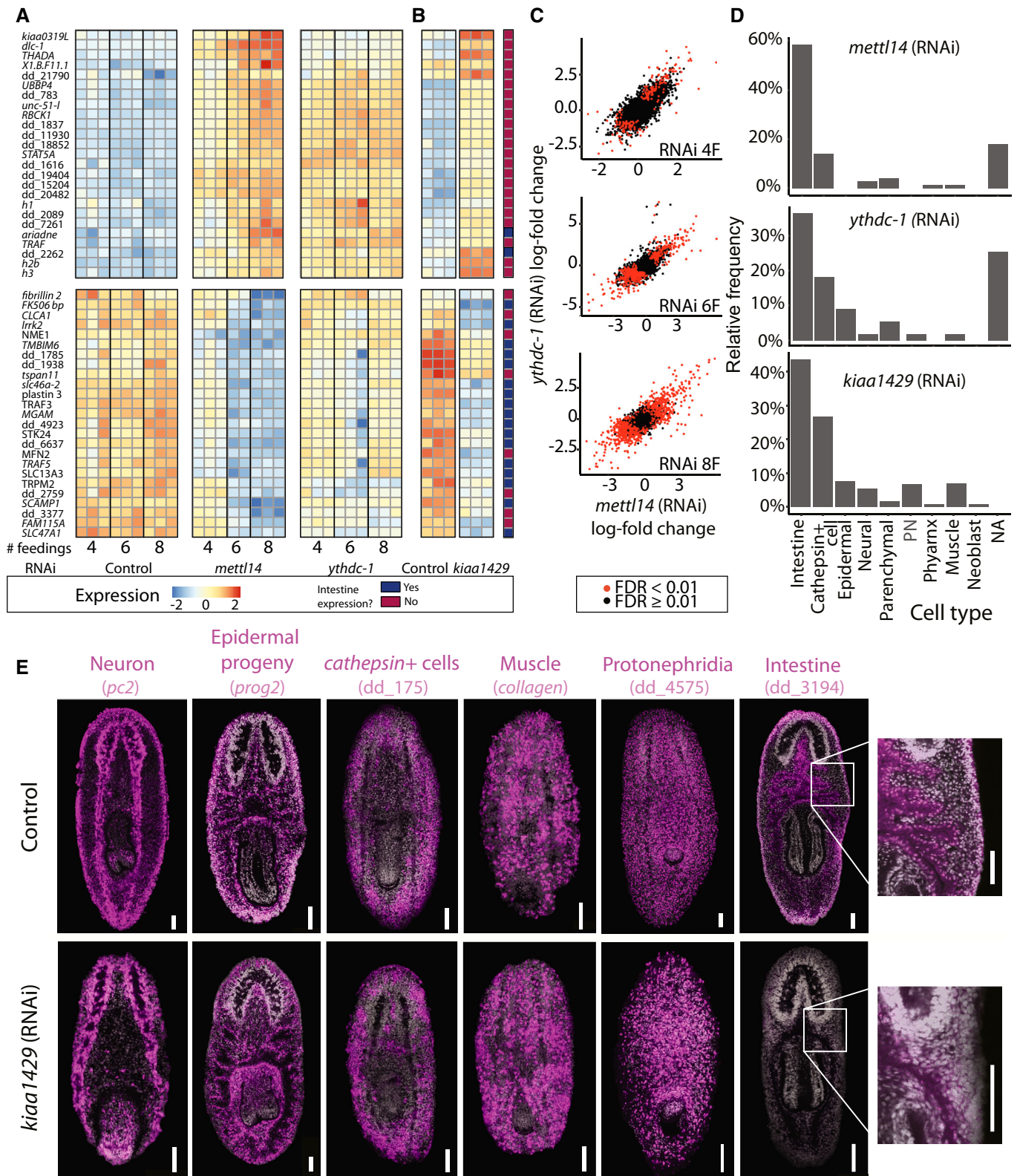


Figure 4.

**Figure 4. Gene expression changes following inhibition of m6A genes.**

- A, B Heatmap of genes that were differentially expressed following inhibition of m6A genes. Shown is the expression of the top 25 overexpressed and 25 underexpressed genes (top and bottom, respectively; Dataset EV2) following six *mettl14* dsRNA feedings, at different conditions and time points. Rows and columns represent genes and samples, respectively. Blue and red, low to high gene expression (row-normalized z-score). Genes that were previously determined to be expressed in the intestine (Fincher et al, 2018) were highlighted in dark blue, or otherwise in dark red.
- C Correlation of gene expression changes between *mettl14* (RNAi) and *ythdc-1* (RNAi) compared to their controls. Each colored dot represents a gene (expression >1 transcripts per million, TPM; red and black, significant and nonsignificant change in gene expression compared to controls, respectively).
- D The proportion of genes that were downregulated following RNAi and were found to be expressed in a single cell type. Shown is an analysis based on the top 300 genes that were downregulated following RNAi (six dsRNA feedings for *mettl14* or *ythdc-1*).
- E FISH for detection of major planarian cell types following inhibition of *kiaa1429* by RNAi using previously established cell-type specific gene expression markers (Fincher et al, 2018). The distribution of most major planarian cell types was comparable between the control (top) and *kiaa1429* (RNAi) animals (bottom). A striking exception was the reduction in intestine cells (right; see Fig EV4E–G for quantification), which severely affected the intestine branching morphology in *kiaa1429* (RNAi) animals. Scale = 100  $\mu$ m.

### m6A indirectly represses polyadenylated histone gene expression and silences repetitive DNA

The reduction in intestine cells together with the increase in the immature progenitor population that we observed by FACS in *kiaa1429* (RNAi) animals suggested that there was a defect in cell production or maturation. We examined the identity of the overexpressed genes in our RNAseq data, which could potentially explain the overabundance of immature progenitors. Previous analysis of cycling planarian cells shows that histone gene expression changes dramatically during neoblast specialization (Labbé et al, 2012). We found that many histone-encoding genes were overexpressed, indicating a broad change to neoblast cell state. For example, seven and eight such genes were upregulated by over twofold in *kiaa1429* (RNAi) and *mettl14* (RNAi) animals, respectively (Fig 5A and B; Dataset EV2). Particularly, *h2b* and *h3* were strongly overexpressed in all conditions (Fig 5A and B; Appendix Fig S1E).

Canonical histone-encoding genes are transcribed without a polyA tail (Dávila López & Samuelsson, 2008). Our RNAseq library preparation protocol selects polyadenylated RNA by using poly-dT beads (Materials and Methods). Therefore, non-polyadenylated RNA should have been vastly excluded from the RNAseq libraries. We hypothesized that the high prevalence of histone-encoding gene transcripts might have represented an aberrant expression of polyadenylated histone isoforms, which were undetectable when the m6A pathway functioned normally.

We tested this hypothesis by searching for polyadenylated histone transcripts in the RNAseq data. Our *kiaa1429* (RNAi) and control libraries were sequenced in a paired-end configuration (Appendix Fig S2A). We reasoned that if *kiaa1429* inhibition resulted in activation of polyadenylated histone transcription, we could detect RNAseq read pairs, where the first read in the pair mapped to a histone gene body, and the second read of the pair had a sequence that includes a polyT, which is the reverse-complement of the polyA tail (Appendix Fig S2A; Materials and Methods). By contrast, in control samples, we expected to find fewer read pairs of this kind (Fig 5C; Appendix Fig S2A–C). Indeed, polyadenylated histone transcripts were detectable almost exclusively in *kiaa1429* (RNAi) RNAseq compared with the control (Fig 5C). For example, we found a >17-fold increase in polyA read mapping to *h2b* following *kiaa1429* (RNAi).

The overexpression of polyadenylated histone RNAs following *kiaa1429* (RNAi) could represent an absolute increase in histone gene expression, or alternatively, a relative increase in polyadenylated histone transcripts compared with non-polyadenylated transcripts.

We compared the total expression of *h2b* in *kiaa1429* (RNAi) and control animals using cDNA produced with random hexamers, which were used to reverse transcribe both polyadenylated and non-polyadenylated RNAs. We found that *h2b* expression levels were essentially identical (Fig 5D; Materials and Methods). This result indicated that the observed increase in *h2b* expression in the RNAseq data resulted from presence of polyadenylated *h2b* transcripts and not from an absolute increase in *h2b* gene expression.

We estimated the proportion of polyadenylated *h2b* transcripts in RNA extracted from control or *kiaa1429* (RNAi) animals. We used cDNA produced with either random hexamers or a poly-dT primer and validated that cDNA production using both methods was similarly efficient (Appendix Fig S2D and E). In control animals, 15.4% of the *h2b* transcripts were polyadenylated. By comparison, following RNAi of *kiaa1429* 80.2% of the *h2b* transcripts were polyadenylated (Fig 5E; Appendix Fig S2F and G). The shift toward production of polyA<sup>+</sup> histone transcripts might reflect changes to cell cycle state, which is often associated with histone transcription (Duronio & Marzluff, 2017; Marzluff & Koreski, 2017). Importantly, we did not detect peaks of m6A in *h2b* and *h3* transcripts (Dataset EV1), which suggested that m6A was not a direct regulator of polyadenylated histone gene expression.

The majority of overexpressed genes following inhibition of the m6A pathway were not associated with a distinct function (Fig 4A and B; Dataset EV2). However, some of the most overexpressed transcripts were annotated as pseudogenes (Dataset EV2). We mapped the RNAseq data to the planarian genome (Rozanski et al, 2019) and inspected regions containing these overexpressed genes. Remarkably, overexpressed genes were highly enriched within genomic clusters (Fig 5F and G). These gene clusters were not expressed in control samples, but were dramatically induced following RNAi (Fig 5F and G; Dataset EV2). Importantly, the intergenic regions in these genomic neighborhoods were almost completely silenced, and therefore, this overexpression was not a consequence of lack of transcriptional regulation over the entire genome segment (Fig 5F and G). Several genes in these clusters had detectable m6A-enriched regions in our m6A-seq2 datasets (Dataset EV1) and encoded ubiquitin-like domain (Dataset EV2). We searched for similar sequences in other planarian transcriptomes (Rozanski et al, 2019) using BLAST and found similar sequences in the *Schmidtea polychroa* transcriptome, but not in other planarian species. We cloned two of these overexpressed genes and performed FISH on *kiaa1429* (RNAi) and control animals (Fig 5H). FISH showed that these genes were indeed expressed only following *kiaa1429* RNAi, validating that expression of m6A genes was required

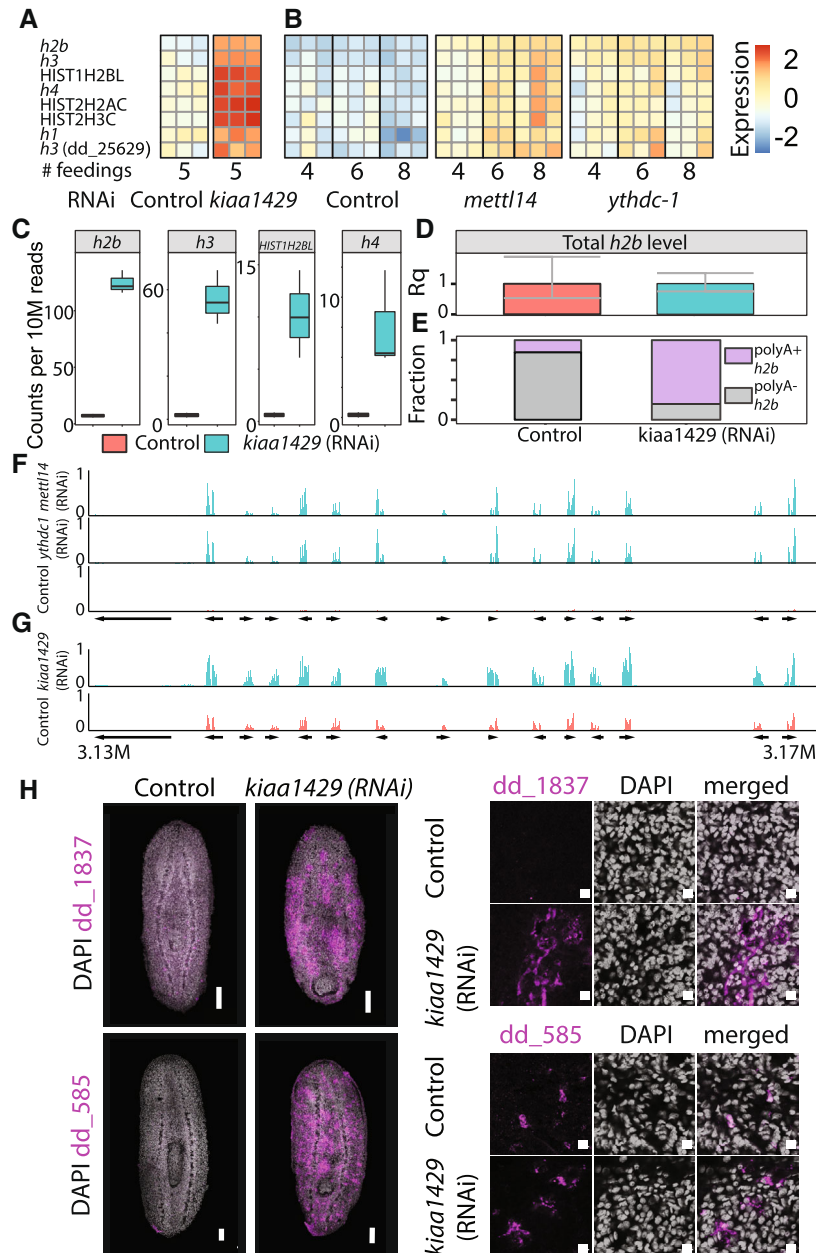


**Figure 5. Overexpression of polyadenylated histone-encoding transcripts.**

- A, B Heatmap showing eight histone-encoding genes that were upregulated following inhibition of m6A-pathway-encoding genes. Rows and columns represent genes and samples, respectively. Blue and red, low to high gene expression (row-normalized z-score).
- C Boxplots showing the normalized number of reads that map to a histone gene body and are paired with a read pair containing a polyA ( $n = 3$  biological replicates). Inhibition of *kiao1429* resulted in a dramatic increase in the mapping to polyA in histone-encoding genes. Boxes represent the IQR, whiskers represent the 1.5 x IQR, and central band represents the median.
- D Quantification of the entire *h2b* transcript pool including polyA<sup>+</sup> and polyA<sup>-</sup> transcripts using qPCR (Materials and Methods). No significant change in the total *h2b* expression was observed following inhibition of *kiao1429*. Error bars represent the 95% confidence interval. Experiment performed in biological triplicates.
- E Comparison of the polyA<sup>+</sup> and polyA<sup>-</sup> *h2b* transcripts showed an overabundance of polyA<sup>+</sup> *h2b* in *kiao1429* (RNAi) animals compared with controls.
- F, G Shown is a summary of gene mapping to a representative overexpressed gene neighborhood (contig: dd\_Smes\_g4\_15). Arrows represent gene annotation, which was extracted from PlanMine (Rozanski et al, 2019). Panels show expression in TPM scaled to 0–1.
- H The overexpression of two representative genes from the upregulated genomic neighborhoods was validated by FISH. Cells expressing these genes were found throughout the animal in sub-epidermal and parenchymal layers (Left, Scale = 100  $\mu$ m); higher magnification shows perinuclear expression (right, scale = 10  $\mu$ m).

for their silencing. We hypothesized that nuclear packaging might be altered. Analysis of nuclear labeling by DAPI of *kiaa1429* (RNAi) and control animals indicated that chromatin density was indeed different (Appendix Fig S3H), with extraneous unlabeled nuclear regions, suggesting a change to nuclear packaging. In summary, inhibition of m6A genes resulted in broad changes to gene expression, including a coordinated overexpression of gene clusters that are normally silenced, together with an overabundance of polyadenylated histone transcripts, indicating an emergence of irregular cell states following inhibition of m6A genes.

### m6A pathway activity regulates cellular maturation

Our results indicated that m6A genes had different roles in different cell populations. We dissected the cell-type-specific roles of m6A genes by using scRNAseq of >20,000 cells isolated from control and *kiaa1429* (RNAi) animals (Figs 6A and EV5A–D; Materials and Methods). Then, we used the Seurat framework (Stuart et al, 2019) and the planarian cell type atlas (Fincher et al, 2018; Plass et al, 2018) for assigning cell type identities for all of the sequenced cells (Dataset EV3). We assigned the cells to 34 major groups, annotated the major planarian cell types, and analyzed gene expression changes following *kiaa1429* (RNAi) for each cell type (Fig 6A and B; Dataset EV3). We focused on several aspects of the m6A depletion phenotype: (i) changes to neoblast gene expression and state; (ii) molecular characterization of the cells expressing the repetitive gene clusters; and (iii) the effect of the RNAi on intestine cells.

The number of *smedwi-1+* cells was similar in control and *kiaa1429* (RNAi) animals. Expression of canonical neoblast genes, such as *smedwi-1+*, *Smed-vasa*, and *Smed-bruli*, was comparable (Fig EV5E; Dataset EV3) indicating that the neoblast population indeed remained intact. By contrast, polyadenylated histone transcripts were broadly overexpressed in highly expressing *smedwi-1* cells following *kiaa1429* inhibition (Fig EV5F), suggesting a broad impact of the RNAi on the neoblast population transcriptional state. Neoblasts express lineage-specific genes during differentiation (Reddien, 2013, 2018). We reclustered the neoblasts and compared lineage-specific gene expression in control and *kiaa1429* (RNAi) cells (Fig EV5G and H). We found two neoblast populations that were reduced by ~40%: intestine-producing neoblast (*nkx-2.2*<sup>+</sup>) and *PLOD*<sup>+</sup> neoblasts (Fig EV5G and H), a class of neoblast that is transcriptionally associated with planarian muscle (Fincher et al, 2018). By contrast, there was an increase of 39–63% in the number of

neural-associated neoblasts, including in the *tspan-1+* neoblasts (Zeng et al, 2018; Raz et al, 2021; Fig EV5G and H). These results suggested that m6A is required for lineage resolution, which if correct would impact the representation of differentiated cell populations. Examination of differentiated cells showed that several lineages were depleted in *kiaa1429* (RNAi) animals (Fig 6B; Dataset EV3). The strongest reduction in lineage representation (≥40%) was detected for intestinal phagocytes, consistent with the reduced representation of intestinal gene expression in bulk RNAseq (Fig 6C and D, and 4A and B, Chi-squared  $P < 1E-15$ ). Using FISH, we saw a reduction in multiple intestinal cell types (Fig 6E; Appendix Fig S3A) and disruption to intestinal morphology (Fincher et al, 2018; Forsthoeft et al, 2020). We quantified the reduction of the intestine markers *dd\_72*, *dd\_115*, and *dd\_888* (Fig 6E; Appendix Fig S3A) by FISH and found a highly significant reduction in the number of *dd\_72*<sup>+</sup> and *dd\_115*<sup>+</sup> cells (Appendix Fig S3A), with only qualitative difference in the expression of *dd\_888*. The intestine lineage was depleted at all stages of the lineage in the scRNAseq data (Figs 6C and D, and EV5I; Chi-squared  $P < 0.001$ ; corrected with Bonferroni's correction), starting at the intestine neoblasts ( $\gamma$ ), continuing with *nkx-2.2*<sup>+</sup>/*smedwi-1*<sup>+</sup> progenitors, and finally with the intestine phagocytes (Figs 6C and D, and EV5I). The dramatic decrease in differentiated cells (~75%) following inhibition of *kiaa1429*, in comparison to a smaller decrease in intestine neoblasts (~50%), might reflect an accumulated defect in cellular production. Indeed, the expression of intestine-specific genes declined progressively in our RNAseq time courses (Fig 4A and B; Dataset EV2). We tested whether there were indeed less recently produced progenitors integrated to the intestine. Recently integrated intestine cells were detected by co-labeling *kiaa1429* (RNAi) and control animals with anti-SMEDWI-1 antibody and with a combination of FISH probes that detects intestine-specific transcription factors (i.e., *nkx-2.2*, *gata4/5/6-1*, and *hnf4*; intestine mix). SMEDWI-1<sup>+</sup>/intestine mix<sup>+</sup> cells were counted in the intestine anterior to the pharynx. We found a significant decrease of >50% (two-way Student's *t*-test  $P = 0.02$ ) in the number of recently integrated progenitors normalized to the size of the animal (Appendix Fig S4B and C). Therefore, despite no detectable change in the number of mitoses, as indicated by H3P and F-ara-EdU labeling (Fig EV4A–D), there was a decrease in the number of newly integrated cells in the intestine.

The increase in neural-associated neoblasts did not result in an overabundance of differentiated neural cells (Fig 6A and B;

**Figure 6. Cell type-specific regulation of gene expression by m6A.**

- A Outline of scRNAseq experiment. Cells were isolated from dissociated animals, purified by FACS and subjected to scRNAseq (top; Materials and Methods). Analysis of cell populations detected in the scRNAseq and visualized by UMAP (dot represents cell, and color represents cluster association). Comparison of scRNAseq of *kiaa1429* (RNAi) and control revealed an expansion of a molecularly defined cell cluster (#20, black arrow).
- B Relative representation of clusters between *kiaa1429* (RNAi) and control animals. Most clusters were similarly represented between samples. However, depletion of phagocytic intestine cells, epidermal progenitors, and expansion of a *kiaa1429* (RNAi) cell cluster was detected (\*>90% difference in detectable the relative cell population size between conditions).
- C, D Analysis of cells from the intestine lineage showed depletion in intestine neoblasts ( $\gamma$ , #6), *nkx-2.2*<sup>+</sup> progenitors (#2), and differentiated intestine cells (#0, #1). Arrow indicates transition to differentiated cell state. Normalized cell count of intestine lineage cells are summarized (bottom).
- E FISH using markers for different intestine cell types (Fincher et al, 2018) demonstrated changes to gene expression and morphological defects following inhibition of *kiaa1429*. Quantification of images found in Appendix Fig S3A. Scale = 100  $\mu$ m.
- F scRNAseq heatmap produced using Seurat (Stuart et al, 2019) of four representative genes from the *kiaa1429* (RNAi)-overexpressed genomic clusters. The major planarian cell types did not express these four genes. By contrast, a *kiaa1429* (RNAi)-specific cell cluster is characterized by high expression of these genes. Rows and columns represent genes and cells, respectively. Purple to yellow, low to high gene expression. Top row shows assignment of cells to cell types based on gene expression (Dataset EV3).

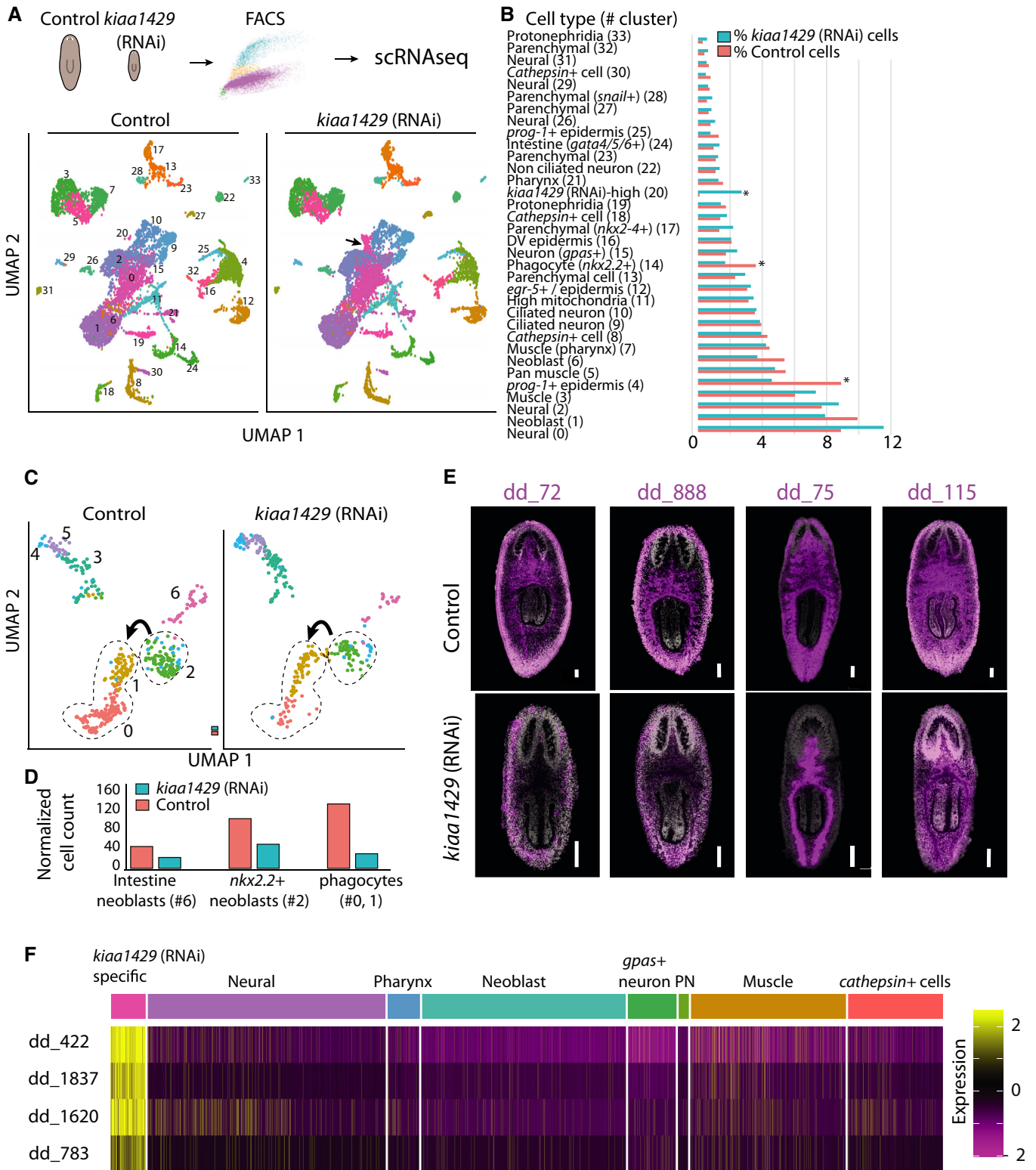


Figure 6.

Dataset EV3). However, we identified a molecularly defined population, which was overrepresented by >27-fold following *kiaa1429* inhibition (Fig 6B). This *kiaa1429* (RNAi)-specific cell cluster had characteristics of post-mitotic progenitors: (i) low-level, but

detectable, expression of *smedwi-1* (Fig EV5J); (ii) expression of genes associated with differentiation (e.g., *xbp-1*, Fig EV5K) (Raz et al, 2021); and (iii) expression of lineage-specific genes that are expressed early in differentiation (Fig EV5L; Dataset EV3). The

scRNAseq analysis indicated that cells in the cluster highly expressed genes that are associated with neurons and glia, such as *Smed-smad6/7-2* and a protocadherin-like gene (*dd\_15376*, gene model SMESG000067388) (González-Sastre *et al*, 2012; Fincher *et al*, 2018; Plass *et al*, 2018; Fig EV5L-M). These *kiaa1429* (RNAi)-specific cells were distinguished from essentially all other cells by expression of the repetitive gene clusters (Fig 6F, Dataset EV3). This result is consistent with the FISH analysis, which demonstrated a body-wide increase in cells expressing genes localized to the repetitive genomic clusters following inhibition of *kiaa1429* (Fig 5H). Taken together, these results support the hypothesis that inhibition of the m6A pathway leads to a decrease in differentiation of several cellular lineages and the expansion of a molecularly defined progenitor population.

### NuRD complex inhibition recapitulates the m6A inhibition phenotype

Multiple lines of evidence indicated that m6A gene expression was required for normal lineage choice and differentiation. m6A is a broad regulator of cellular function, and the inhibition of the m6A pathway could produce this phenotype by affecting other processes directly or indirectly. To better understand the mechanistic basis for the m6A phenotypes, we searched for conditions that induce similar changes to gene expression. We mapped 1,080 published planarian RNAseq libraries to the planarian transcriptome (Rozanski *et al*, 2019) and then compared gene expression changes in the published data with the RNAseq data that we generated following inhibition of the m6A genes (Appendix Fig S4; Materials and Methods; Table EV1).

Remarkably, this analysis revealed that inhibition of *Smed-CHD4*, which encodes a canonical component of the Nucleosome Remodeling and Deacetylase complex (NuRD), recapitulated all of the major aspects of the m6A phenotype (Dataset EV4): (i) overexpression of the repetitive gene clusters that were identified following RNAi of m6A genes (Fig 7A); (ii) *CHD4* RNAi resulted in overexpression of polyadenylated histone-encoding transcripts (Fig 7B and D; Appendix Fig S5A), as we observed in *kiaa1429* (RNAi) animals; (iii) The expression of *smedwi-1* was unperturbed, indicating that the neoblast population size was unchanged (Appendix Fig S5A); and (iv) Strikingly, *CHD4* (RNAi) animals had reduced intestine gene expression, including transcription factors that are essential for intestinal cell differentiation, morphogenesis, and function (Forsthoefel *et al*, 2012, 2020), as we observed following inhibition of the m6A genes (Fig 7E). We inhibited a different NuRD complex-encoding gene, *RbAp48*, which also resulted in an overexpression of polyadenylated *h2b* transcripts (Appendix Fig S5B). This further suggested that the molecular similarities detected following inhibition of m6A genes and *CHD4* could be generalizable to other NuRD components, which is consistent with the roles of NuRD in transcriptional regulation (Basta & Rauchman, 2015). Interestingly, we analyzed previously published gene expression data from human and mouse of NuRD inhibition by shRNA or by conditional deletion and identified an overexpression of histone genes, such as *h2b* (Wilczewski *et al*, 2018; Marques *et al*, 2020; Appendix Fig S5C and D; Materials and Methods). This indicated that regulation of histone gene expression by *CHD4* is found in diverse animals.

We considered potential associations of m6A and NuRD, which might explain the similarities in the phenotypes: (i) NuRD and m6A

regulate similar processes independently; (ii) NuRD regulates m6A gene expression or m6A pathway activity; or (iii) m6A regulates NuRD. We first examined whether NuRD activity was required for the expression of m6A genes and found that the expression of m6A genes was unperturbed following inhibition of *CHD4* (Dataset EV4). Then, we tested whether *CHD4* was required for m6A formation and found that inhibition of *CHD4* did not deplete m6A (Fig 7F), indicating that NuRD is not necessary for m6A formation. Therefore, NuRD activity is unlikely to be required for the activity of the MTC. We next tested whether m6A genes regulated NuRD gene expression. Inhibition of m6A genes did not result in downregulation of *CHD4* or any other NuRD-encoding components (Dataset EV2; Materials and Methods). This, of course, does not eliminate the possibility that the production or activity of one or more of NuRD components is regulated posttranscriptionally by m6A. Interestingly, *CHD4* (RNAi) animals developed phenotypes more rapidly than following inhibition of m6A genes. For example, lysis and changes to gene expression were observed following three RNAi feedings, in contrast to the 8–10 RNAi feedings that were required for lysis following *mettl14* (RNAi). It is possible that inhibition of the m6A pathway progressively deteriorates NuRD activity, directly or indirectly. However, it is also possible that the m6A pathway and NuRD function independently and that their inhibition results in similar phenotypes.

## Discussion

m6A has been implicated in myriad regulatory roles in diverse biological systems (Dominissini *et al*, 2012; Batista *et al*, 2014; Kan *et al*, 2017; Zhang *et al*, 2017). Given the essentiality of the MTC, research in mammalian systems has been limited to studying the role of this complex either in cell lines (Dominissini *et al*, 2012; Batista *et al*, 2014; Geula *et al*, 2015; Liu *et al*, 2020b), or upon selective depletion of this complex in specific tissues or cell types, which has provided a partial and fragmented view on the roles played by this modification. Obtaining a global view on the functions and underlying mechanisms of action of m6A can hugely benefit from systemic, organism-wide perturbations of the MTC, as have been conducted in a highly limited number of model organisms to date, most of which in species evolutionary distant from human such as yeast and plants (Schwartz *et al*, 2013, 2014; Kan *et al*, 2017; Bhat *et al*, 2018; Baumgarten *et al*, 2019). Our study adds to these efforts and introduces a systematic analysis of the MTC function in an adult Lophotrochozoan, planarian, which is a widely used model for studying regeneration.

Among the major questions for which we lacked a general understanding to date is the nature of the relationship between methylation writers and readers. All organisms surveyed to date have only a single “writer” machinery, but organisms vary widely in terms of the number of readers that they have, ranging from one detected reader in yeast (Schwartz *et al*, 2013) to 13 in plants (Reichel *et al*, 2019). Oftentimes, deletion of the writers is associated with a severe phenotype, whereas readers are associated with much milder defects. In some cases, this has been attributed to redundancy between readers (Kontur *et al*, 2020; Zaccara & Jaffrey, 2020; Lasman *et al*, 2020b), but in most cases it cannot be ruled out that the full function of the writers is not mediated by readers, but instead by other machineries (Reichel *et al*, 2019), potentially also methylation-independent ones. In this

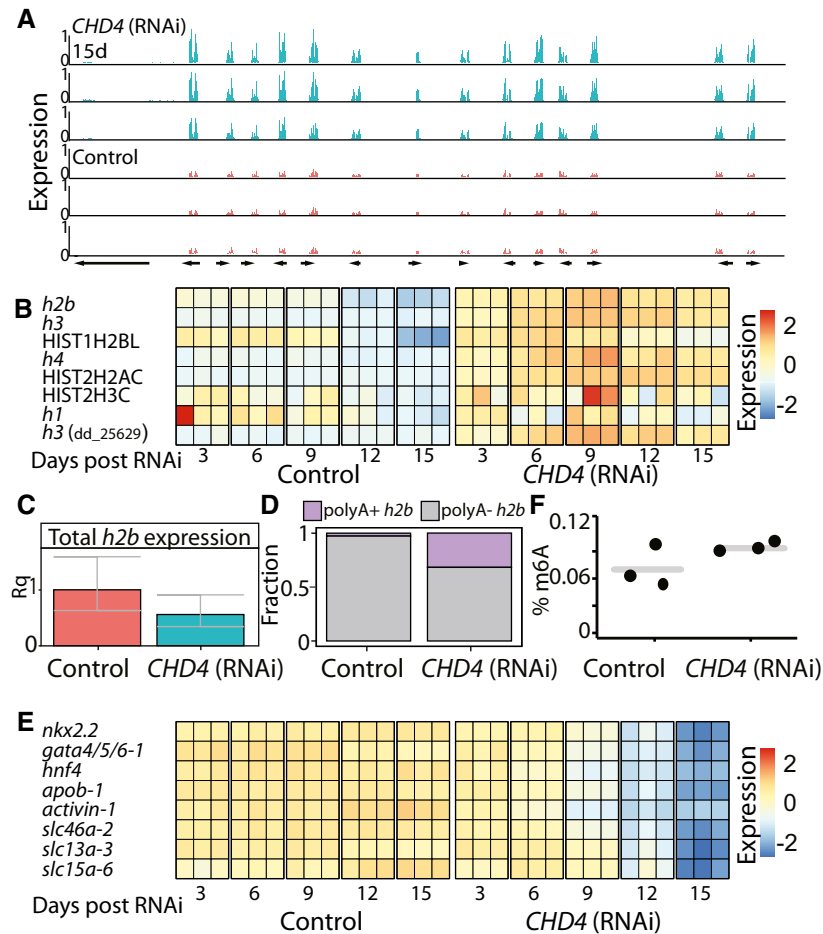


**Figure 7. Inhibition of *CHD4* recapitulates effects of the m6A-pathway inhibition.**

- A Overexpressed gene neighborhood (contig: dd\_Smes\_g4\_15:3.13–3.17 Mbp). Shown is the normalized and scaled gene expression in three *CHD4* (RNAi) samples, 15 days post feedings (top, blue) and in three corresponding control samples (bottom, red).
- B Heatmap showing the eight histone-encoding genes that were upregulated following inhibition of *CHD4*, at different time points, in published dataset (Tu *et al*, 2015). Rows and columns represent genes and samples, respectively. Blue and red, low to high gene expression (row normalized z-score).
- C Quantification of the entire *h2b* transcript pool including polyA<sup>+</sup> and polyA<sup>-</sup> transcripts using qPCR (Materials and Methods). No significant change in the absolute expression of *h2b* inhibition of *CHD4* (Bonferroni corrected Student's *t*-test). Error bars represent the 95% confidence interval (At least two biological replicates, with two technical replicates for each biological replicate).
- D Comparison of the polyA<sup>+</sup> and polyA<sup>-</sup> *h2b* expression level shows an increase in polyA<sup>+</sup> *h2b* in *CHD4* (RNAi) animals compared to control animals.
- E Heatmap showing the gene expression levels of intestine-specific TFs and genes following *CHD4* RNAi at different time points. Rows and columns represent genes and samples, respectively. Blue and red, low and high gene expression (row normalized z-score).
- F Quantification of m6A on RNA isolated from *CHD4* (RNAi) or control animals showed no significant change in abundance of m6A methylation (Student's *t*-test).

regard, our findings mark a relatively rare exception—alongside with a previous report in *Drosophila* (Kan *et al*, 2017), and some recently reported findings in mouse embryonic stem cells (mESC)—in which the full phenotype associated with inhibition of a writer is phenocopied via inhibition of one reader. This strongly suggests a methylation-dependent function and demonstrates that this function is likely to be mediated entirely via one reader. In parallel, these findings raise questions regarding the role played by the additional readers encoded in the planarian genome, whose disruption fails to give rise to a discernible phenotype. The absence of a phenotype may either be technical, or due to functional redundancy, and will be assessed in future studies.

We profiled the distribution of m6A in the planarian transcriptome and identified 7,600 enriched regions in a diversity of cell

types. Our profiling approach included mRNA enrichment and was therefore focused on the detection of m6A enrichment in mRNAs. The m6A-enriched regions were found mostly near the 3'-end of the transcripts, as previously reported in other systems (Domissini *et al*, 2012; Schwartz *et al*, 2014). This suggested that the role of m6A in planarians is similar to other systems. However, we identified a unique feature of planarian m6A-enriched regions: they are longer, on average, than reported m6A-enriched regions in other organisms (Liu *et al*, 2020c). This might be explained by lack of antibody specificity, yet we did not observe similar outcomes in our yeast samples. The detection of longer m6A-enriched regions might be a consequence of individual RNA molecules having multiple methylated adenosine sites in proximity, which could be therefore detected as a broad m6A-rich region. Single-nucleotide resolution-

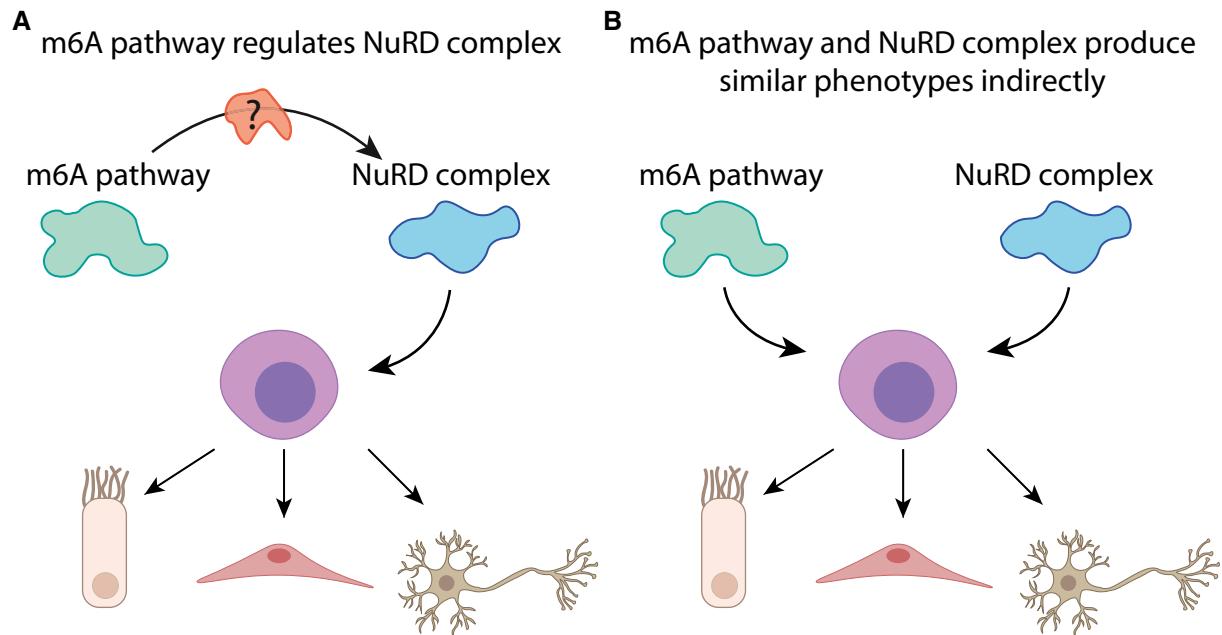


**Figure 8. Potential models for interaction of m6A and NuRD.**

Shown are two models demonstrating the potential regulatory activity of m6A on neoblast differentiation.

A m6A might regulate neoblast homeostasis by directly regulating NuRD or through a mediator that modulates NuRD function.

B In the alternative model m6A and NuRD regulate similar processes, in parallel, without an association between the pathways.

based approaches for detection of m6A, such as miCLIP (Grozhiik *et al.*, 2017), could further elucidate these findings.

Importantly, we found essentially identical phenotypes following inhibition of the MTC-encoding genes *mettl14*, *kiaa1429*, and of the putative m6A-reader, *ythdc-1*. The phenotypes were reminiscent of a stem cell deficiency in a regenerative adult organism (Wagner *et al.*, 2012): decline in animal size, failure to regenerate, and eventually death. In a developmental system, similar defects would be detrimental. Indeed, elimination of m6A in developmental contexts has revealed that m6A is critical for early development, cell maturation, and differentiation (Batista *et al.*, 2014; Geula *et al.*, 2015; Lasman *et al.*, 2020a).

Integration of our analysis of the m6A phenotypes showed that m6A is required for production of the planarian intestine with more minor impact on other lineages. Defects in differentiation to certain lineages, but not necessarily to all, have been reported in embryonic stem cells (ESC) (Batista *et al.*, 2014). However, in addition to the defect in differentiation, the lack of m6A in planarians resulted in an emergence of a molecularly defined cell type throughout the planarian body. These cells were undetectable in control animals, and they lacked characteristics of neoblasts: they expressed low levels of neoblast markers and had different morphology. Moreover, these abnormal cells expressed several genes that are broadly expressed in neural progenitors, such as a protocadherin-like gene (*dd\_15376*, gene model SMESG000067388) and *Smed-SMAD6/7-2*. The scRNAseq clustering analysis positioned these cells adjacent to other neural cells, yet further *in vivo* evidence is required for determining their identity. Therefore, m6A, in planarians, is required for resolving the identity of the differentiating progenitors.

Recently, an analysis of mESCs has found that deletion of *Mettl3* promotes an open state of the chromatin by regulating a class of

chromatin associated RNAs (Liu *et al.*, 2020a). In addition, *Mettl3* regulates self-renewal of neural stem cells by destabilizing transcripts that encode histone modifiers (Wang *et al.*, 2018). Analysis of planarian nuclei following inhibition of *kiaa1429* suggested that chromatin packaging was altered, which similarly to the findings in the mammalian system, may have profound effect on chromatin accessibility, and could be tested in future experiments. Moreover, we found that some of the most highly overexpressed genes, following inhibition of m6A genes, were localized to distinct genomic regions characterized by repetitive DNA. These regions were not expressed in control animals. Incorporation of the planarian cell type gene expression atlas (Fincher *et al.*, 2018) with our m6A mapping data showed that 248 neoblast-associated transcripts are highly methylated, including many transcriptional regulators (Dataset EV1). Most importantly, inhibition of *CHD4*, a component of the NuRD complex, has revealed striking molecular similarities, including reduction in intestine cells and upregulation of the repetitive genomic regions. Interestingly, p66, a DNA-binding component of the NuRD complex, is known to suppress the production of photoreceptor neurons in planarians, suggesting of a link between NuRD and production of the neural lineage (Vásquez-Doorman & Petersen, 2016). Potentially, m6A could affect the activity of chromatin regulators (Fig ), or alternatively, regulate similar processes indirectly (Fig 8B).

We did not detect NuRD complex genes that were highly methylated by m6A. Furthermore, inhibition of the m6A pathway did not affect NuRD complex gene expression. Similarly, inhibition of *CHD4* did not affect the levels of m6A on planarian RNAs and did not result in a change to gene expression of canonical MTC components. Therefore, the striking similarities between the roles of m6A and NuRD, in planarians, could not be ascribed to simple transcriptional

regulation. We therefore suggest two different models for the regulatory association of m6A and NuRD (Fig 8). In the first, m6A is required for proper activity of NuRD, potentially through a mediating molecule that is dependent on m6A methylation (Fig 8A). Alternatively, m6A and NuRD regulate similar processes, such as chromatin accessibility or emergence of a new cell state (Benham-Pyle et al, 2021), independently (Fig 8B). Further study of neoblast-specific RNAs that are modified by m6A might reveal the identity of a mediating molecule or distinguish between the two models.

In summary, we have mapped the distribution of m6A in the planarian transcriptome, characterized the roles of RNA-level modifications in planarian tissue maintenance and regeneration, and demonstrated that m6A is indispensable for regulation of neoblast homeostasis. Our study lays the foundation to a mechanistic analysis of planarian gene expression regulation and consequently a system-level understanding of planarian stem cell homeostasis.

## Materials and Methods

### Identification of putative m6A-pathway and NuRD complex encoding genes

Sequences of genes encoding the MTC complex were extracted from the human, yeast, and fly genomes. Reciprocal BLAST search was performed with tblastx (Camacho et al, 2009) with e-value  $<1 \times 10^{-5}$  using the planarian transcriptome assembly (Liu et al, 2013). Putative reader-encoding genes were identified by searching YTH domains *in silico* using hmmscan V3 with parameters [--noali --cut\_nc --acc --notextw] (Eddy, 2011). The resultant sequences were then searched in other planarian species in PlanMine (Rozanski et al, 2019). Contig IDs predicted to encode the planarian NuRD complex (GO:0016581) were extracted from PlanMine (Rozanski et al, 2019).

### Synthesis of double-stranded RNA for RNAi experiments and RNAi feedings

Double-stranded RNA (dsRNA) was synthesized as previously described (Rouhana et al, 2013). Briefly, *in vitro* transcription (IVT) templates were prepared by PCR amplification of cloned target sequences using primers with 5' flanking T7 promoter sequences. dsRNA was synthesized using the TranscriptAid T7 High Yield Transcription Kit (CAT K0441; Thermo Scientific). Reactions were incubated overnight at 37°C and then supplemented with RNase-free DNase for 30 min. RNA was purified by ethanol precipitation and finally resuspended in 25  $\mu$ l of ddH<sub>2</sub>O. RNA was analyzed on 1% agarose gel and quantified by Qubit 4 (Thermo scientific) for validating a concentration higher than 5  $\mu$ g/ $\mu$ l. Animals were starved for at least 7 days prior to RNAi experiments. *Schmidtea mediterranea*, asexual, were used for all experiments. Animals were fed with dsRNA mixed with beef liver twice a week as previously described (Wurtzel et al, 2017).

### cDNA synthesis from total RNA or polyadenylated RNA for qPCR

RNA samples were converted to cDNA and amplified using RevertAid H Minus First Strand cDNA Synthesis Kit (Thermo scientific; K1631). Random hexamers or oligo(dT) primers were used for

obtaining cDNA from total RNA or from polyadenylated RNA, respectively. Resultant cDNA was used for qPCR analysis.

### Fluorescence-activated cell sorting (FACS)

Planarians were cut into small fragments using a blade. Tissue fragments were collected into calcium-free, magnesium-free medium plus 0.1% BSA (CMFB) and dissociated with collagenase 1 (1 mg/ml) by pipetting for 5–10 min. To reduce clumping at downstream steps, dissociated cells were strained through a 40  $\mu$ m filter. Cells were centrifuged at 315 g for 5 min at 4°C and resuspended in CMFB containing Hoechst 33342 (40  $\mu$ l/ml) for 45 min at RT in the dark. Before loading into FACSaria II flow cytometer (Becton Dickinson), cells were labeled with propidium iodide (5  $\mu$ g/ml) for cell viability detection. FACS gating was performed as previously described for planarian cell populations (Hayashi et al, 2006).

### Preparation of RNA sequencing libraries

RNAseq libraries for *mettl14* (RNAi), *ythdc-1* (RNAi), and their control samples were prepared using Kapa stranded mRNAseq (KK8420) according to the manufacturer's protocol.

### Planarian fixation for whole-mount assays

Fixation was performed as previously described (King & Newmark, 2013). Animals were killed with 5% N-acetyl-cysteine in PBS for 5 min, then fixed with 4% formaldehyde in PBSTx 0.1 for 20 min. Animals were then washed in PBSTx, 50:50 PBSTx:methanol and stored in methanol at -20°C until further analysis.

### Whole-mount fluorescence *in situ* hybridization

Fluorescence *in situ* hybridization (FISH) was performed as previously described (King & Newmark, 2013) with minor modifications. Briefly, fixed animals were bleached and treated with proteinase K (2  $\mu$ g/ml) in 1 $\times$  PBSTx. Following overnight hybridizations, samples were washed twice in pre-hyb solution, 1:1 pre-hyb-2 $\times$  SSC, 2 $\times$  SSC, 0.2 $\times$  SSC, PBSTx. Subsequently, blocking was performed in 0.5% Roche Western Blocking Reagent and 5% inactivated horse serum in 1 $\times$  PBSTx. Animals were incubated in an antibody overnight at 4°C (anti-DIG-POD, 1:1,500). Post-antibody washes and tyramide development were performed as previously described (King & Newmark, 2013). Specimens were counterstained with DAPI overnight at 4°C (Sigma, 1  $\mu$ g/ml in PBSTx).

### Metabolic labeling by F-ara-EdU

Animals were soaked for 16 h in 2.5 mg/ml F-ara-EdU (Sigma-Aldrich T511293) diluted in planarian water. Then, animals were fixed in NAC and bleached with formamide and H<sub>2</sub>O<sub>2</sub> for 2 h on a light table. Animals were treated with 0.2  $\mu$ g/ml Proteinase K for 10 min, 4% FA for 10 min, and were then washed three times in 3% PBSB (PBS supplemented with 3% BSA). Click reaction was performed using baseclick kit (cat. Back-edu488) and was followed by nuclear staining (DAPI, 1:5,000) overnight in 4°C. Samples were washed three times in PBSTx (0.1%) for 10 min and then mounted for imaging.

### H3P labeling

H3P labeling was performed based on published protocols (Wenemoser & Reddien, 2010; LoCascio *et al*, 2017) on animals following fixation with NAC. Briefly, following fixation blocking was performed with 10% heat inactivated horse serum (HIHS). Anti-phospho-Histone H3 Antibody (sigma 04817) was added 1:100 overnight in 4°C. Samples were washed seven times with PBSTx (0.1% triton) for 20 min and were labeled using goat anti-rabbit-HRP secondary antibody (Abcam ab6721, 1:300) overnight at 4°C in block. Samples were developed using rhodamine tyramide diluted 1:1,000 in PBSTi.

### Image processing for figure assembly

Fluorescent and confocal images were acquired using confocal microscope (Zeiss LSM800). Live images were taken using stereomicroscope (Leica S9i). Images were cropped and rotated, and masks of planarian outline were defined in Adobe Photoshop using the lasso and the object selection tools. Background color, outside the defined mask, was standardized in Adobe Photoshop or in Adobe Illustrator as light blue and black for live and fluorescent images, respectively.

### Cell counting following FISH in whole-mount planarian samples

Images of samples labeled FISH, immunofluorescence, or F-ara-Edu were collected using a confocal microscope (Zeiss LSM800). Cell counting was performed on controls and experimental condition. Positive cells were counted using the “Cell Counter” component in ImageJ (Rueden *et al*, 2017), and the normalized positive cell count was calculated by measuring the area used for cell counting in each animal. Unless mentioned otherwise, the cells were counted in a rectangle starting at the posterior part of the brain and ending at the anterior of the pharynx in ventrally mounted animals.

### Cell counting in microscopy images

Counting of H3P+ cells was performed in a rectangle starting anterior to the pharynx and ending at the posterior end of the brain, excluding the epidermis, which had nonspecific labeling background, and includes no neoblasts. Cell counting was performed in z-stack images in slices of 4 μm. Cell count was normalized to the area of quantification.

Counting of intestinal phagocytes was performed on *mettl14* (RNAi) and *ythdc-1* (RNAi) animals. Intestinal phagocytes were labeled using a specific marker by FISH (dd\_3194). Animals were imaged by confocal microscopy, and the z-position showing the largest number of intestinal phagocytes anterior to the pharynx, as determined by two researchers, was selected for counting. Cells were counted using the Cell Counter module in ImageJ (Schindelin *et al*, 2012; Rueden *et al*, 2017). Then, the length of the intestine branches was measured by tracing the intestine based on DAPI labeling next to the intestine lumen by using the segmented line tool in ImageJ. The normalized number of cells per micron of intestine branch was calculated based on these measurements.

F-ara-Edu+ cells were counted in a rectangle starting anterior to the pharynx and ending at the posterior end of the brain, in a

subepidermal layer that does not include intestine branches, which had nonspecific labeling background. The number of F-ara-Edu+ cells was normalized to the area of the region.

### Statistical analysis

Statistical tests were performed using GraphPad Prism (v9.2) and the R (v4.0) environment. Differentially expressed genes were determined using edgeR (3.30.3) with functions glmQLFit and glmQLFTest (McCarthy *et al*, 2012) and with DESeq2 (Love *et al*, 2014). Threshold for considering an effect significant in hypothesis testing was 0.05, unless stated otherwise. Multiple hypothesis testing was controlled using the Benjamini–Hochberg Procedure or by applying the Bonferroni correction.

### Gene cloning and transformation

Genes were amplified from planarian cDNA using gene-specific primers and cloned into pGEM-t vector using the manufacturer’s protocol (Promega; CAT #A1360). Vectors were transformed into *E. coli* TOP10 (Thermo Fisher Scientific) by the heat-shock method. Briefly, 100 μl of bacteria was mixed with 5 μl of each of the cloned vectors, incubated on ice for 30 min, and then placed at 42°C for 45 s. Then, the transformed bacteria were supplemented with 350 μl of SOC medium, and following 1 h of recovery at 37°C, the bacteria were plated on agarose plates containing 1:2,000 Ampicillin, 1:200 Isopropylthio-β-D-galactoside (IPTG), and 1:625 5-bromo-4-chloro-3-indolyl-β-D-galactopyranoside (X-gal). Colonies were grown overnight at 37°C, and colonies were screened by colony PCR using M13F and M13R primers with the following PCR program: (i) 5 min at 95°C; (ii) 34 cycles of 45 s at 95°C, 60 s at 55°C, and 2:30 min at 72°C; (iii) 10 min at 72°C; (iv) hold at 10°C. Reactions were analyzed by gel electrophoresis, and correctly sized gene products were grown overnight in Luria Broth (LB) medium, supplemented with 1:2,000 Ampicillin at 37°C. Plasmids were purified from overnight cultures with the NucleoSpin Plasmid Miniprep Kit (Macherey-Nagel; CAT #740588). Cloned gene sequences were sequenced by Sanger sequencing.

### Measurement of m6A level in purified RNA

m6A RNA methylation level was measured by an m6A RNA methylation assay kit (Abcam, ab185912) following the manufacturer’s protocol. Total of 200 ng of RNA isolated from control, *mettl14* (RNAi), and *kiaa1429* (RNAi) animals was used to determine the fraction of m6A in the RNA. Separately, m6A was measured on polyadenylated RNA and non-polyadenylated RNA from wild-type planarians. PolyA<sup>+</sup> RNA was separated from polyA<sup>-</sup> RNA using the NEXTFLEX Poly(A) Beads 2.0 kit (PerkinElmer). Following anti-m6A-antibody capture, the absorbance was measured at 450 nm using a microplate reader, and the percentage of m6A in the RNA was calculated using the kit supplied controls.

### RNA extraction

Samples were collected into 700 μl TRI Reagent (Sigma; CAT #9424) and then homogenized using 0.5 mm zirconium beads in a bead beating homogenizer (Allsheng; Bioprep-24) for two cycles of 45 s

at 3,500 RPM followed by incubation of 5 min at room temperature. Then, 140  $\mu$ l of chloroform was added to each tube. Tubes were shaken for 15 s and then incubated at room temperature for 3 min. Then, samples were centrifuged at 4°C, 12,000 g for 25 min. The upper phase was separated into a new tube. Then, 500  $\mu$ l of isopropanol was added, and tubes were inverted five times and then incubated for 10 min at room temperature. Samples were centrifuged at 4°C (12,000 g) for 45 min. The supernatant was removed and the pellet was washed twice with 75% EtOH, centrifuged at 4°C 7,500 g for 5 min, and air-dried for 10 min. RNA was resuspended in 30  $\mu$ l of H<sub>2</sub>O. RNA concentration was measured by Qubit (Invitrogen; Q33226) according to the manufacturer's protocol.

### mRNA m6A immunoprecipitation library preparation

m6A immunoprecipitation was performed as previously described (Dierks et al, 2021). RNA samples were extracted from *kiaa1429* (RNAi) animals or control, *unc22* (RNAi), animals in triplicates, following five dsRNA feedings. Each replicate included at least nine animals. RNA was quantified using Qubit (Invitrogen, Q33226), and 20  $\mu$ g of *kiaa1429* (RNAi) and 30  $\mu$ g of *unc22* (RNAi) RNA were used per sample per replicate. mRNA was enriched by two rounds of polyA selection (Dynabeads, CAT #61011) according to the manufacturer's protocol. mRNA-enriched samples were quantified by spectrophotometry (SpectraMax QuickDrop, Molecular Devices) and fragmented by RNA Fragmentation Reagents (Ambion, AM8740) for 2 min. Fragmented RNA was purified by MyOne Silane beads (Thermo, 37002D). Then, the purified RNA was treated with Turbo DNase (Thermo Fisher Scientific, AM2238), and the RNA was treated with FastAP (Fermentas, EF0651) and T4 PNK (CAT M0201L), according to the m6A pulldown protocol. Each RNA sample was barcoded by ligation to a unique 3' adapter, which was flanked by a universal sequence that was used subsequently for reverse transcription. Then, the barcoded RNA samples were pooled by mixing, and 10% of the pooled sample volume was separated and used as control (input) for the m6A pulldown experiment. Immunoprecipitation of m6A was performed by using an anti-m6A antibody (Synaptic Systems) according to protocol. RNAseq libraries were prepared from the immunoprecipitated RNA and input RNA, separately, following the published protocol (Dierks et al, 2021). Library integrity was analyzed by fragment analysis (Agilent TapeStation 4000). Libraries were sequenced on an Illumina (NextSeq 550) machine at the Tel Aviv University NGS unit.

### Processing of m6A-seq2 library data

m6A-seq2 libraries were pooled and sequenced in paired-end mode (Dierks et al, 2021). The resultant sequencing reads were then demultiplexed (i.e., separated to individual libraries) based on an inline library adapter that was ligated to each library according to the protocol (Dierks et al, 2021). Demultiplexing was performed by using cutadapt --pair-filter = any --minimum-length 24 (Martin, 2011) by supplying internal barcode sequences, followed by trimming of the 10 nt sequence of the barcode from the barcoded sequencing read (Read #2). The resultant fastq files were pre-processed and mapped to the planarian transcriptome as described in the RNAseq library analysis method section. m6A-enriched regions (m6a peaks) were determined using MeTPeak with default

parameters (Cui et al, 2016). Plots of m6A peak profiles and peak heatmaps were produced using deepTools2 (Ramírez et al, 2016). Peak profiles were generated by merging BAM files of the three replicates of the control or *kiaa1429* (RNAi) libraries using the samtools merge command (Li et al, 2009). Then, mapping coverage was calculated for the merged control or *kiaa1429* (RNAi) BAM file using the deepTools2 command bamCoverage with parameters [--normalizeUsing RPKM --binSize 30]. The resultant files were then used for generating peak matrices with the computeMatrix scale-regions command, which was followed by producing the profile plots with the plotProfile command with parameters [--plotType lines --perGroup]. Peak heatmaps were produced by taking all of the detectable m6A peaks that were enriched by at least fivefold in the pulldown libraries over the input. Then, the computeMatrix scale-regions command was used followed by the command plotHeatmap with parameters [--kmeans 3 --t "#2166 ac,#d1e5f0,#ef8a62,#b2182b"]. Mixed species m6A-seq2 experiment was performed by using RNA from yeast (*Saccharomyces cerevisiae* sk1) and from planarian (Fig EV3). RNA was mixed following RNA isolation and polyA-enrichment, prior to other processing to reduce biases that are associated with handling of RNA. Two pools of RNA were produced, in duplicates by mixing 80% of planarian RNA with 20% of yeast RNA: (i) Control planarian RNA mixed with RNA from *S. cerevisiae* lacking m6A, due to genetic mutation *Ime4Δ/Δ/Ndt80Δ/Δ* (Dierks et al, 2021); and (ii) planarian RNA from *kiaa1429* (RNAi) animals, which have a reduced m6A level, with RNA from *S. cerevisiae* having high level of m6A because genetic background (*Ndt80Δ/Δ*) (Dierks et al, 2021). The pools were then processed according to the m6A-seq2 protocol. Briefly, the barcoded planarian-yeast pools were combined, and immunoprecipitation of m6A was performed using an anti-m6A antibody. Library preparation and Illumina sequencing were performed according to the m6A-seq2 protocol. Sequencing reads were assigned to respective planarian-yeast pool based on the sequence of their molecular 3'-end barcode (Appendix Table S3) and were then assigned to the planarian or yeast genome by mapping the sequences of each pool to a combined genome sequence of planarian (Rozanski et al, 2019), and *S. cerevisiae* (Dierks et al, 2021), or by mapping reads to a combined transcriptome sequence of planarian and the *S. cerevisiae* genome sequence. Enrichment in m6A sequence was performed by MeTPeak with default parameters (Cui et al, 2016), and motif finding was performed on regions enriched with m6A that are shorter than 250 bp using HOMER with parameters [-size given -len 5 using the 500 most enriched m6A regions] (Heinz et al, 2010), and using an orthogonal m6A-associated k-mer enrichment detection strategy (Schwartz et al, 2014; Dierks et al, 2021).

### qPCR analysis of gene expression following RNAi

RNA concentration of each sample was measured using Qubit 4 fluorometer (Invitrogen; Q33226). cDNA synthesis was performed on 1  $\mu$ g of RNA from each sample using RevertAid H Minus First Strand cDNA Synthesis Kit (Thermo scientific; K1631), following these steps: RNA template was mixed with an oligo-dT primer and then incubated at 65°C for 5 min. Then, cDNA synthesis proceeded according to the manufacturer's protocol: samples were incubated at 42°C for 60 min and then at 70°C for 5 min. The cDNA sample concentrations were normalized to 1 ng/ $\mu$ l. The expression of the

target genes was measured using the QuantStudio 3 Real-Time PCR system (Applied Biosystems) using the following program [95°C (20 s), 40 cycles (95°C 1 s, 60°C 20 s)], with two technical replicates per sample and at least two biological replicates per sample. The relative gene expression fold-change was calculated by the  $\Delta\Delta C_t$  method with *gapdh* used as an endogenous control. Forward and reverse primers were designed for each target gene. Primer efficiency was tested prior to the experiment by using the standard curve method for five decreasing cDNA concentrations.

#### Analysis of RNA sequencing gene expression changes

RNAseq sequencing files were preprocessed by trimming the Illumina adapter sequences using trimmomatic V0.38 (Bolger *et al*, 2014) [ILLUMINACLIP:TruSeq3-PE.fa:2:30:10:2:keepBothReads LEADING:0 TRAILING:3 SLIDINGWINDOW:4:15 MINLEN:30]. Then, the trimmed RNAseq sequences were mapped to the planarian transcriptome (ddV4) (Liu *et al*, 2013) and genome (Rozanski *et al*, 2019) using bowtie2 (Langmead & Salzberg, 2012) and HISAT2 (Kim *et al*, 2019), respectively. Mapping of transcriptome assembly contig IDs to planarian gene models was fetched from PlanMine (Rozanski *et al*, 2019). Gene expression matrix was then produced using the featureCounts command from the subread-2.0 package with parameters [-M -s 0] (Liao *et al*, 2014) for the analyzed RNAseq libraries. Differentially expressed genes were detected using edgeR (3.30.3) with functions glmQLFit and glmQLFTest (McCarthy *et al*, 2012), and with DESeq2 (1.28.1) (Love *et al*, 2014).

#### Detection of polyadenylated transcripts in RNAseq data

Paired-end RNAseq libraries were preprocessed with trimmomatic V0.38 (Bolger *et al*, 2014) with parameters [ILLUMINACLIP:TruSeq3-PE.fa:2:30:10:2:keepBothReads LEADING:0 TRAILING:3 SLIDINGWINDOW:4:15 MINLEN:30]. For RNAseq libraries, reads in the Read #2 files were derived from antisense paired-reads. Sequencing reads from Read #2 files, which contained homopolymers (>10 nt), were discarded, but their read pair (Read #1) was kept. The retained Read #1 file was then mapped to the planarian transcriptome (Rozanski *et al*, 2019) using bowtie2 V2.3.5.1 with default parameters (Langmead & Salzberg, 2012). Reads that mapped to histone-encoding genes were isolated from the resultant read mapping BAM file (Li *et al*, 2009). Then, the unmapped read-pair (Read #2) of the isolated mapped-reads (Read #1) was selected from the raw paired-end RNAseq fastq files. An unmapped Read #2 sequence that included at least 10 consecutive T nucleotides (i.e., the reverse complement of the polyA) was counted as a polyA-containing read. The number of polyA-containing reads was summarized per library and normalized by the library size.

#### Quantification of polyadenylated *h2b* fraction by qPCR

RNA was isolated from *kiaa1429* (RNAi) and from control animals. Purified RNA was converted to cDNA by using random hexamers or poly dT primers. The cDNA samples concentrations were normalized to 1 ng/ $\mu$ l. qPCR was performed using QuantStudio 3 Real-Time PCR system (Applied Biosystems) with the following settings [95°C (20 s), 40 cycles (95°C 1 s, 60°C 20 s)], with two technical replicates per sample and at least two biological

replicates per sample. The relative fold gene expression was calculated by the  $\Delta\Delta C_t$  method with *gapdh* used as the endogenous control.

#### Preparation of scRNAseq libraries following *kiaa1429* (RNAi)

Animals were fed five times with *unc22* (control) and *kiaa1429* dsRNA. Animals were starved for a week following RNAi feedings. Cells were purified for scRNAseq from either control or *kiaa1429* (RNAi) animals by FACS using hoechst-labeling, as previously described (Fincher *et al*, 2018). Cells were counted and collected by centrifugation (300 g, 5 min). The supernatant was discarded, and the cells were resuspended in 1 $\times$  PBS with 0.5% BSA to achieve an optimal cell concentration of approximately 1,000 cells per  $\mu$ l. Cells were counted automatically using the Invitrogen Countess II (Thermo Fisher Scientific), and the cell viability was assessed by labeling with trypan blue (0.4%) and counting positive cells.

Libraries were then prepared at the Genomic Research Unit at Tel Aviv University using the 10 $\times$  Genomics Chromium Controller in conjunction with the single-cell 3' v3.1 kit, protocol revision D. Briefly, cell suspensions were diluted in nuclease-free water according to the manufacturer's protocol to 10,000 cells in each sample. The cDNA synthesis, barcoding, and library preparation were carried out according to the manufacturer's instructions. cDNA libraries were sequenced on Illumina NextSeq 550 at Tel Aviv University.

#### Systematic gene expression analysis of published planarian RNAseq data

A table of previously published planarian high-throughput sequencing libraries was extracted from the Sequence Read Archive (Leinonen *et al*, 2011). The table was manually curated and libraries were divided into biological groups, in each experiment, based on the library description in the Short Read Archive (Table EV1). Then, each library was downloaded using sra-tools (Leinonen *et al*, 2011) and was processed on a computational cluster using the computational pipeline used for the RNAseq libraries that were produced in this project. The resultant differential gene expression analysis tables, which were produced for the previously published planarian data, were used for searching for the genes that were differentially expressed in the libraries produced in this project with the following thresholds (FDR <0.0001,  $\log_2 > 1$  or  $\log_2 < -1$ ). We tested a range of parameters for calling differentially expressed genes in the published dataset (FDR range from 0.1 to 1E-10; minimal gene expression 1–20 transcript per million, TPM) and searched for overlap of gene expression with our dataset. The significance of overlap of differentially expressed genes was robust to these thresholds. To minimize spurious potential correlations, we used conservative thresholds requiring corrected FDR < 1E-5 and TPM > 10, in order to include a gene in the list of differentially expressed genes for this analysis. The *CHD4* (RNAi) libraries at 9, 12, 15 days following RNAi had the most significant overlap of differentially expressed genes with the list of differentially expressed genes in our datasets with *P*-value, estimated by hypergeometric hypothesis test, of <1E-15 and often *P*-value <1E-60, with the highest ranking of overlap (Appendix Fig S4A). For example, 31 out of the top 50 differentially expressed genes in

following *mettl14* (RNAi) were differentially expressed in the *CHD4* (RNAi) 15 days condition, compared with a median overlap of four differentially expressed genes in all of the tested libraries. Furthermore, we selected up to 200 genes with the lowest adjusted *P*-value, which meet the thresholds for differential expression, from each condition and computed the Jaccard similarity coefficient (JI). The median JI between our libraries and each of the libraries in this analysis was  $<0.02$ , compared with  $JI >0.14$  at 9 and 15 days following *CHD4* (RNAi) with the *kiaa1429* (RNAi) library. The JI for the *CHD4* (RNAi) and our libraries was significantly larger than JIs calculated for the other groups as estimated by two-sided Wilcoxon rank sum ( $P = 0.0002$ ).

### Analysis of human and mouse gene expression data from *CHD4* inhibition or conditional knockout

RNAseq libraries of control and conditional knockout of *CHD4* from mouse (Wilczewski et al, 2018) and from control and shRNA-treated samples against *CHD4* from human (Marques et al, 2020) were obtained from the sequence read archive using the `fasterq-dump` command (Leinonen et al, 2011). The raw fastq files were trimmed using Trimmomatic-0.38 (Bolger et al, 2014) [ILLUMINACLIP:TruSeq3-PE.fa:2:30:10:2:keepBothReads LEADING:0 TRAILING:3 SLIDINGWINDOW:4:15 MINLEN:30]. Mouse and human samples were mapped to genome assemblies mm10 and hg38, respectively, using HISAT2 with default parameters (Kim et al, 2019). Gene expression was estimated using featureCounts (Liao et al, 2014) using the included human or mouse annotations. Finally, differential gene expression analysis was performed using DESeq2 (Love et al, 2014) with the DESeq pipeline. Resultant differential gene expression tables were annotated with the bioconductor annotation packages `org.Mm.eg.db` and `org.Hs.eg.db`, for mouse and human, respectively (Huber et al, 2015).

## Data availability

High-throughput sequencing data produced in this project were deposited to the Sequence Read Archive (Leinonen et al, 2011). The data are available under BioProject accession [PRJNA747686](https://www.ncbi.nlm.nih.gov/bioproject/PRJNA747686).

**Expanded View** for this article is available online.

## Acknowledgements

We thank Sarit Edelheit for support with the m6A-seq2 protocol. We thank Rami Khosravi for assistance with scRNAseq, and Hila Kobo for assistance with Illumina sequencing at the Tel Aviv University core facilities. We thank Jenny Barboj-Smoljarenko for assistance in illustration. We thank the Wurtzel lab for critical input. O.W. is supported by the Israel Science Foundation (grant 2039/18) and the European Research Council (no. 853640). O.W. is a Zuckerman Faculty Scholar. P.W.R. acknowledges NIH support (R01GM080639). P.W.R. is an investigator of the Howard Hughes Medical Institute and an associate member of the Broad Institute of Harvard, and MIT. S.S. is supported by the European Research Council (ERC) under the European Union's Horizon 2020 research and innovation program (grant agreement No. 714023). A.R.B. was supported by grant F32-GM128411 by the National Institute of General Medical Sciences.

## Author contributions

**Yael Dagan:** Conceptualization; data curation; formal analysis; investigation; visualization; methodology; writing – original draft; writing – review and editing. **Yarden Yesharim:** Conceptualization; data curation; formal analysis; investigation; visualization; methodology; writing – original draft; writing – review and editing. **Ashley R Bonneau:** Conceptualization; investigation; methodology. **Tamar Frankovits:** Data curation; investigation. **Schraga Schwartz:** Software; investigation; methodology; writing – review and editing. **Peter W Reddien:** Conceptualization; resources; formal analysis; funding acquisition; writing – review and editing. **Omri Wurtzel:** Conceptualization; resources; data curation; software; formal analysis; supervision; funding acquisition; investigation; visualization; methodology; writing – original draft; project administration; writing – review and editing.

## Disclosure and competing interests statement

The authors declare that they have no conflict of interest.

## References

- Adler CE, Sánchez Alvarado A (2015) Types or states? Cellular dynamics and regenerative potential. *Trends Cell Biol* 25: 687–696
- Basta J, Rauchman M (2015) The nucleosome remodeling and deacetylase complex in development and disease. *Transl Res* 165: 36–47
- Batista PJ, Molinie B, Wang J, Qu K, Zhang J, Li L, Bouley DM, Lujan E, Haddad B, Daneshvar K et al (2014) M(6)a RNA modification controls cell fate transition in mammalian embryonic stem cells. *Cell Stem Cell* 15: 707–719
- Baumgarten S, Bryant JM, Sinha A, Reyser T, Preiser PR, Dedon PC, Scherf A (2019) Transcriptome-wide dynamics of extensive m6A mRNA methylation during *Plasmodium falciparum* blood-stage development. *Nat Microbiol* 4: 2246–2259
- Benham-Pyle BW, Brewster CE, Kent AM, Mann FG, Chen S, Scott AR, Box AC, Sánchez Alvarado A (2021) Identification of rare, transient post-mitotic cell states that are induced by injury and required for whole-body regeneration in *Schmidtea mediterranea*. *Nat Cell Biol* 23: 939–952
- Bhat SS, Bielewicz D, Jarmolowski A, Szwejkowska-Kulinska Z (2018) N<sup>6</sup>-methyladenosine (m<sup>6</sup>A): revisiting the old with focus on new, an *Arabidopsis thaliana* centered review. *Genes (Basel)* 9: 596
- Bolger AM, Lohse M, Usadel B (2014) Trimmomatic: a flexible trimmer for Illumina sequence data. *Bioinformatics* 30: 2114–2120
- Camacho C, Coulouris G, Avagyan V, Ma N, Papadopoulos J, Bealer K, Madden TL (2009) BLAST+: architecture and applications. *BMC Bioinformatics* 10: 421
- Cui X, Meng J, Zhang S, Chen Y, Huang Y (2016) A novel algorithm for calling mRNA m6A peaks by modeling biological variances in MeRIP-seq data. *Bioinformatics* 32: i378–i385
- Dávila López M, Samuelsson T (2008) Early evolution of histone mRNA 3' end processing. *RNA* 14: 1–10
- Dierks D, Garcia-Campos MA, Uzonyi A, Safra M, Edelheit S, Rossi A, Sideri T, Varier RA, Brandis A, Stelzer Y et al (2021) Multiplexed profiling facilitates robust m6A quantification at site, gene and sample resolution. *Nat Methods* 18: 1060–1067
- Dominissini D, Moshitch-Moshkovitz S, Schwartz S, Salmon-Divon M, Ungar L, Osenberg S, Cesarkas K, Jacob-Hirsch J, Amariglio N, Kupiec M et al (2012) Topology of the human and mouse m6A RNA methylomes revealed by m6A-seq. *Nature* 485: 201–206

- Duncan EM, Chitsazan AD, Seidel CW, Sánchez Alvarado A (2015) Set1 and MLL1/2 target distinct sets of functionally different genomic loci *in vivo*. *Cell Rep* 13: 2741–2755
- Duronio RJ, Marzluff WF (2017) Coordinating cell cycle-regulated histone gene expression through assembly and function of the Histone Locus Body. *RNA Biol* 14: 726–738
- Eddy SR (2011) Accelerated profile HMM searches. *PLoS Comput Biol* 7: e1002195
- Fincher CT, Wurtzel O, de Hoog T, Kravarik KM, Reddien PW (2018) Cell type transcriptome atlas for the planarian *Schmidtea mediterranea*. *Science* 360: eaaq1736
- Forsthoefel DJ, James NP, Escobar DJ, Stary JM, Vieira AP, Waters FA, Newmark PA (2012) An RNAi screen reveals intestinal regulators of branching morphogenesis, differentiation, and stem cell proliferation in planarians. *Dev Cell* 23: 691–704
- Forsthoefel DJ, Cejda NI, Khan UW, Newmark PA (2020) Cell-type diversity and regionalized gene expression in the planarian intestine. *eLife* 9: e52613
- Geula S, Moshitch-Moshkovitz S, Dominissini D, Mansour AA, Kol N, Salmon-Divon M, Hershkovitz V, Peer E, Mor N, Manor YS et al (2015) m6A mRNA methylation facilitates resolution of naïve pluripotency toward differentiation. *Science* 347: 1002–1006
- González-Sastre A, Molina MD, Saló E (2012) Inhibitory Smads and bone morphogenetic protein (BMP) modulate anterior photoreceptor cell number during planarian eye regeneration. *Int J Dev Biol* 56: 155–163
- Grozhi AV, Linder B, Olarerin-George AO, Jaffrey SR (2017) Mapping m6A at individual-nucleotide resolution using crosslinking and immunoprecipitation (miCLIP). *Methods Mol Biol* 1562: 55–78
- Guo T, Peters AHFM, Newmark PA (2006) A *Bruno-like* gene is required for stem cell maintenance in planarians. *Dev Cell* 11: 159–169
- Hayashi T, Asami M, Higuchi S, Shibata N, Agata K (2006) Isolation of planarian X-ray-sensitive stem cells by fluorescence-activated cell sorting. *Dev Growth Differ* 48: 371–380
- Heinz S, Benner C, Spann N, Bertolino E, Lin YC, Laslo P, Cheng JX, Murre C, Singh H, Glass CK (2010) Simple combinations of lineage-determining transcription factors prime *cis*-regulatory elements required for macrophage and B cell identities. *Mol Cell* 38: 576–589
- Hongay CF, Orr-Weaver TL (2011) *Drosophila* inducer of MEiosis 4 (IME4) is required for notch signaling during oogenesis. *Proc Natl Acad Sci USA* 108: 14855–14860
- Huber W, Carey VJ, Gentleman R, Anders S, Carlson M, Carvalho BS, Bravo HC, Davis S, Gatto L, Girke T et al (2015) Orchestrating high-throughput genomic analysis with Bioconductor. *Nat Methods* 12: 115–121
- Kan L, Grozhi AV, Vedanayagam J, Patil DP, Pang N, Lim K-S, Huang Y-C, Joseph B, Lin C-J, Despic V et al (2017) The m6A pathway facilitates sex determination in *Drosophila*. *Nat Commun* 8: 15737
- Kim D, Paggi JM, Park C, Bennett C, Salzberg SL (2019) Graph-based genome alignment and genotyping with HISAT2 and HISAT-genotype. *Nat Biotechnol* 37: 907–915
- King RS, Newmark PA (2013) In situ hybridization protocol for enhanced detection of gene expression in the planarian *Schmidtea mediterranea*. *BMC Dev Biol* 13: 8
- Kontur C, Jeong M, Cifuentes D, Giraldez AJ (2020) Ythdf m6A readers function redundantly during zebrafish development. *Cell Rep* 33: 108598
- Labbé RM, Irimia M, Currie KW, Lin A, Zhu SJ, Brown DDR, Ross EJ, Voisin V, Bader GD, Blencowe BJ et al (2012) A comparative transcriptomic analysis reveals conserved features of stem cell pluripotency in planarians and mammals. *Stem Cells* 30: 1734–1745
- Langmead B, Salzberg SL (2012) Fast gapped-read alignment with bowtie 2. *Nat Methods* 9: 357–359
- Lasman L, Hanna JH, Novershtern N (2020a) Role of m6A in embryonic stem cell differentiation and in gametogenesis. *Epigenomes* 4: 5
- Lasman L, Krupalnik V, Viukov S, Mor N, Aguilera-Castrejón A, Schneir D, Bayerl J, Mizrahi O, Peles S, Tawil S et al (2020b) Context-dependent functional compensation between Ythdf m6A reader proteins. *Genes Dev* 34: 1373–1391
- Lee Y, Choe J, Park OH, Kim YK (2020) Molecular mechanisms driving mRNA degradation by m6A modification. *Trends Genet* 36: 177–188
- Leinonen R, Sugawara H, Shumway M, International Nucleotide Sequence Database Collaboration (2011) The sequence read archive. *Nucleic Acids Res* 39: D19–D21
- Lence T, Soller M, Roignant J-Y (2017) A fly view on the roles and mechanisms of the m6A mRNA modification and its players. *RNA Biol* 14: 1232–1240
- Li H, Handsaker B, Wysoker A, Fennell T, Ruan J, Homer N, Marth G, Abecasis G, Durbin R, 1000 Genome Project Data Processing Subgroup (2009) The Sequence Alignment/Map format and SAMtools. *Bioinformatics* 25: 2078–2079
- Liao Y, Smyth GK, Shi W (2014) featureCounts: an efficient general purpose program for assigning sequence reads to genomic features. *Bioinformatics* 30: 923–930
- Lin AYT, Pearson BJ (2014) Planarian *yorkie/YAP* functions to integrate adult stem cell proliferation, organ homeostasis and maintenance of axial patterning. *Development* 141: 1197–1208
- Linder B, Grozhi AV, Olarerin-George AO, Meydan C, Mason CE, Jaffrey SR (2015) Single-nucleotide-resolution mapping of m6A and m6Am throughout the transcriptome. *Nat Methods* 12: 767–772
- Liu SY, Selck C, Friedrich B, Lutz R, Vila-Farré M, Dahl A, Brandl H, Lakshmanaperumal N, Henry I, Rink JC (2013) Reactivating head regrowth in a regeneration-deficient planarian species. *Nature* 500: 81–84
- Liu J, Dou X, Chen C, Chen C, Liu C, Xu MM, Zhao S, Shen B, Gao Y, Han D et al (2020a) N6-methyladenosine of chromosome-associated regulatory RNA regulates chromatin state and transcription. *Science* 367: 580–586
- Liu J, Li K, Cai J, Zhang M, Zhang X, Xiong X, Meng H, Xu X, Huang Z, Peng J et al (2020b) Landscape and regulation of m6A and m6Am methylome across human and mouse tissues. *Mol Cell* 77: 426–440.e6
- Liu S, Zhu A, He C, Chen M (2020c) REPIC: a database for exploring the N6-methyladenosine methylome. *Genome Biol* 21: 100
- LoCascio SA, Lapan SW, Reddien PW (2017) Eye absence does not regulate planarian stem cells during eye regeneration. *Dev Cell* 40: 381–391.e3
- Love MI, Huber W, Anders S (2014) Moderated estimation of fold change and dispersion for RNA-seq data with DESeq2. *Genome Biol* 15: 550
- Marques JG, Gryder BE, Pavlovic B, Chung Y, Ngo QA, Frommelt F, Gstaiger M, Song Y, Benischke K, Laubscher D et al (2020) NuRD subunit CHD4 regulates super-enhancer accessibility in rhabdomyosarcoma and represents a general tumor dependency. *Elife* 9: e54993
- Martin M (2011) Cutadapt removes adapter sequences from high-throughput sequencing reads. *EMBnet J* 17: 10
- Marzluff WF, Koreski KP (2017) Birth and death of histone mRNAs. *Trends Genet* 33: 745–759
- McCarthy DJ, Chen Y, Smyth GK (2012) Differential expression analysis of multifactor RNA-Seq experiments with respect to biological variation. *Nucleic Acids Res* 40: 4288–4297
- Molinaro AM, Pearson BJ (2018) Myths vs. FACS: what do we know about planarian stem cell lineages? *Int J Dev Biol* 62: 527–535

- Patil DP, Pickering BF, Jaffrey SR (2018) Reading m6A in the transcriptome: m6A-binding proteins. *Trends Cell Biol* 28: 113–127
- Plass M, Solana J, Wolf FA, Ayoub S, Misios A, Glažar P, Obermayer B, Theis FJ, Kocks C, Rajewsky N (2018) Cell type atlas and lineage tree of a whole complex animal by single-cell transcriptomics. *Science* 360: eaaq1723
- Ramírez F, Ryan DP, Grüning B, Bhardwaj V, Kilpert F, Richter AS, Heyne S, Dündar F, Manke T (2016) deepTools2: a next generation web server for deep-sequencing data analysis. *Nucleic Acids Res* 44: W160–W165
- Raz AA, Wurtzel O, Reddien PW (2021) Planarian stem cells specify fate yet retain potency during the cell cycle. *Cell Stem Cell* 28: 1307–1322.e5
- Reddien PW (2013) Specialized progenitors and regeneration. *Development* 140: 951–957
- Reddien PW (2018) The cellular and molecular basis for planarian regeneration. *Cell* 175: 327–345
- Reddien PW, Oviedo NJ, Jennings JR, Jenkin JC, Sánchez Alvarado A (2005) SMEDWI-2 is a PIWI-like protein that regulates planarian stem cells. *Science* 310: 1327–1330
- Reichel M, Köster T, Staiger D (2019) Marking RNA: m6A writers, readers, and functions in Arabidopsis. *J Mol Cell Biol* 11: 899–910
- Rink JC (2013) Stem cell systems and regeneration in planaria. *Dev Genes Evol* 223: 67–84
- Rouhana L, Weiss JA, Forsthoefel DJ, Lee H, King RS, Inoue T, Shibata N, Agata K, Newmark PA (2013) RNA interference by feeding *in vitro*-synthesized double-stranded RNA to planarians: methodology and dynamics. *Dev Dyn* 242: 718–730
- Rozanski A, Moon H, Brandl H, Martín-Durán JM, Grohme MA, Hüttner K, Bartscherer K, Henry I, Rink JC (2019) PlanMine 3.0-improvements to a mineable resource of flatworm biology and biodiversity. *Nucleic Acids Res* 47: D812–D820
- Rueden CT, Schindelin J, Hiner MC, DeZonia BE, Walter AE, Arena ET, Eliceiri KW (2017) ImageJ2: ImageJ for the next generation of scientific image data. *BMC Bioinformatics* 18: 529
- Růžička K, Zhang M, Campilho A, Bodi Z, Kashif M, Saleh M, Eeckhout D, El-Showk S, Li H, Zhong S et al (2017) Identification of factors required for m6A mRNA methylation in Arabidopsis reveals a role for the conserved E3 ubiquitin ligase HAKAI. *New Phytol* 215: 157–172
- Sahu S, Sridhar D, Abnave P, Kosaka N, Dattani A, Thompson JM, Hill MA, Aboobaker A (2021) Ongoing repair of migration-coupled DNA damage allows planarian adult stem cells to reach wound sites. *eLife* 10: e63779
- Schindelin J, Arganda-Carreras I, Frise E, Kaynig V, Longair M, Pietzsch T, Preibisch S, Rueden C, Saalfeld S, Schmid B et al (2012) Fiji: an open-source platform for biological-image analysis. *Nat Methods* 9: 676–682
- Schwartz S, Agarwala SD, Mumbach MR, Jovanovic M, Mertins P, Shishkin A, Tabach Y, Mikkelsen TS, Satija R, Ruvkun G et al (2013) High-resolution mapping reveals a conserved, widespread, dynamic mRNA methylation program in yeast meiosis. *Cell* 155: 1409–1421
- Schwartz S, Mumbach MR, Jovanovic M, Wang T, Maciag K, Bushkin GG, Mertins P, Ter-Ovanesyan D, Habib N, Cacchiarelli D et al (2014) Perturbation of m6A writers reveals two distinct classes of mRNA methylation at internal and 5' sites. *Cell Rep* 8: 284–296
- Scimone ML, Meisel J, Reddien PW (2010) The mi-2-like *Smed-CHD4* gene is required for stem cell differentiation in the planarian *Schmidtea mediterranea*. *Development* 137: 1231–1241
- Solana J, Kao D, Mihaylova Y, Jaber-Hijazi F, Malla S, Wilson R, Aboobaker A (2012) Defining the molecular profile of planarian pluripotent stem cells using a combinatorial RNAseq, RNA interference and irradiation approach. *Genome Biol* 13: R19
- Stuart T, Butler A, Hoffman P, Hafemeister C, Papalexi E, Mauck WM, Hao Y, Stoeckius M, Smibert P, Satija R (2019) Comprehensive integration of single-cell data. *Cell* 177: 1888–1902.e21
- Tu KC, Cheng L-C, T K Vu H, Lange JJ, McKinney SA, Seidel CW, Sánchez Alvarado A (2015) Egr-5 is a post-mitotic regulator of planarian epidermal differentiation. *eLife* 4: e10501
- Wagner DE, Ho JJ, Reddien PW (2012) Genetic regulators of a pluripotent adult stem cell system in planarians identified by RNAi and clonal analysis. *Cell Stem Cell* 10: 299–311
- Wang Y, Li Y, Yue M, Wang J, Kumar S, Wechsler-Reya RJ, Zhang Z, Ogawa Y, Kellis M, Duester G et al (2018) N6-methyladenosine RNA modification regulates embryonic neural stem cell self-renewal through histone modifications. *Nat Neurosci* 21: 195–206
- Wenemoser D, Reddien PW (2010) Planarian regeneration involves distinct stem cell responses to wounds and tissue absence. *Dev Biol* 344: 979–991
- Wilczewski CM, Hepperla AJ, Shimbo T, Wasson L, Robbe ZL, Davis IJ, Wade PA, Conlon FL (2018) CHD4 and the NuRD complex directly control cardiac sarcomere formation. *Proc Natl Acad Sci USA* 115: 6727–6732
- van Wolfswinkel JC, Wagner DE, Reddien PW (2014) Single-cell analysis reveals functionally distinct classes within the planarian stem cell compartment. *Cell Stem Cell* 15: 326–339
- Vásquez-Doorman C, Petersen CP (2016) The NuRD complex component p66 suppresses photoreceptor neuron regeneration in planarians. *Regeneration* 3: 168–178
- Wurtzel O, Cote LE, Poirier A, Satija R, Regev A, Reddien PW (2015) A generic and cell-type-specific wound response precedes regeneration in planarians. *Dev Cell* 35: 632–645
- Wurtzel O, Oderberg IM, Reddien PW (2017) Planarian epidermal stem cells respond to positional cues to promote cell-type diversity. *Dev Cell* 40: 491–504.e5
- Yang Y, Hsu PJ, Chen Y-S, Yang Y-G (2018) Dynamic transcriptomic m6A decoration: writers, erasers, readers and functions in RNA metabolism. *Cell Res* 28: 616–624
- Zaccara S, Jaffrey SR (2020) A unified model for the function of YTHDF proteins in regulating m6A-modified mRNA. *Cell* 181: 1582–1595.e18
- Zeng A, Li H, Guo L, Gao X, McKinney S, Wang Y, Yu Z, Park J, Semerad C, Ross E et al (2018) Prospectively isolated Tetraspanin+ neoblasts are adult pluripotent stem cells underlying planaria regeneration. *Cell* 173: 1593–1608.e20
- Zhang C, Chen Y, Sun B, Wang L, Yang Y, Ma D, Lv J, Heng J, Ding Y, Xue Y et al (2017) m6A modulates haematopoietic stem and progenitor cell specification. *Nature* 549: 273–276
- Zheng Z, Zhang L, Cui X-L, Yu X, Hsu PJ, Lyu R, Tan H, Mandal M, Zhang M, Sun H-L et al (2020) Control of early B cell development by the RNA N6-Methyladenosine methylation. *Cell Rep* 31: 107819
- Zhu SJ, Hallows SE, Currie KW, Xu C, Pearson BJ (2015) A *mex3* homolog is required for differentiation during planarian stem cell lineage development. *eLife* 4: e07025



**License:** This is an open access article under the terms of the [Creative Commons Attribution-NonCommercial-NoDerivs](https://creativecommons.org/licenses/by-nc-nd/4.0/) License, which permits use and distribution in any medium, provided the original work is properly cited, the use is non-commercial and no modifications or adaptations are made.

## Expanded View Figures

### Figure EV1. m6A genes are conserved and functional in planarians.

- A Conservation of the genes encoding the MTC is shown across diversity of organisms. Annotation for *A. thaliana* was obtained from a previous analysis (Růžička et al, 2017).
- B Domain analysis of putative YTH-domain (red block) containing genes.
- C, D The gene expression of planarian MTC and reader-encoding genes, across different cell types and lineages, was extracted from the planarian scRNAseq resource (Plass et al, 2018) (blue to red, low and high expression levels, respectively). The expression of MTC-encoding genes is widespread in different cell types, including in the stem cell compartment (black arrow, indicated in the *mettl3* panel). The expression of reader-encoding genes is not widespread, except for *ythdc-1*, which is expressed across multiple cell types and conditions.
- E Inhibition of m6A genes resulted in lysis of the animals and eventually death. Shown are representative control and *kiaa1429* (RNAi) animals. Scale = 1 mm.
- F Inhibition of m6A genes resulted in defects in food uptake. Shown are animals following feeding with calf liver mixed with a red food color. Control animals show normal food uptake (top) compared with *kiaa1429* (RNAi) animals, which stopped eating. Size measurements were performed on separate animals, which were subjected to the same RNAi treatment. Student's *t*-test; \*\*\*\**P* < 0.0001. Scale = 1 mm.
- G Inhibition of *mettl14* and *ythdc-1* by RNAi has resulted in size reduction. Shown are representative images (left) and measurement of animal sizes following nine RNAi feedings. Significance was calculated using one-way ANOVA followed by Dunnett's multiple comparison test; \*\*\**P* < 0.001; \**P* < 0.05. Scale = 1 mm.
- H qPCR analysis showed that the gene expression of *mettl3* (top) and *wtap* (bottom) is not downregulated significantly following RNAi, which could likely explain the lack of penetrant phenotypes in these conditions. Error bars indicate the 95% confidence interval. Samples include two technical replicates and at least two biological replicates.
- I Schematic of the design of two non-overlapping gene fragments that were used for synthesis of dsRNA targeting the *kiaa1429* gene. The sequence used for the experiments presented in the manuscript was labeled "original *kiaa1429* clone."
- J dsRNA that was produced using a second cloned fragment of *kiaa1429*, labeled "non-overlapping *kiaa1429* (RNAi)," produced phenotypes that were similar to the phenotypes observed in a non-overlapping clone. This further indicated that the *kiaa1429* (RNAi) phenotype resulted from inhibition of *kiaa1429* gene expression and not because of an off-target effect of the RNAi. Student's *t*-test \*\*\**P* < 0.001. Scale = 1 mm.

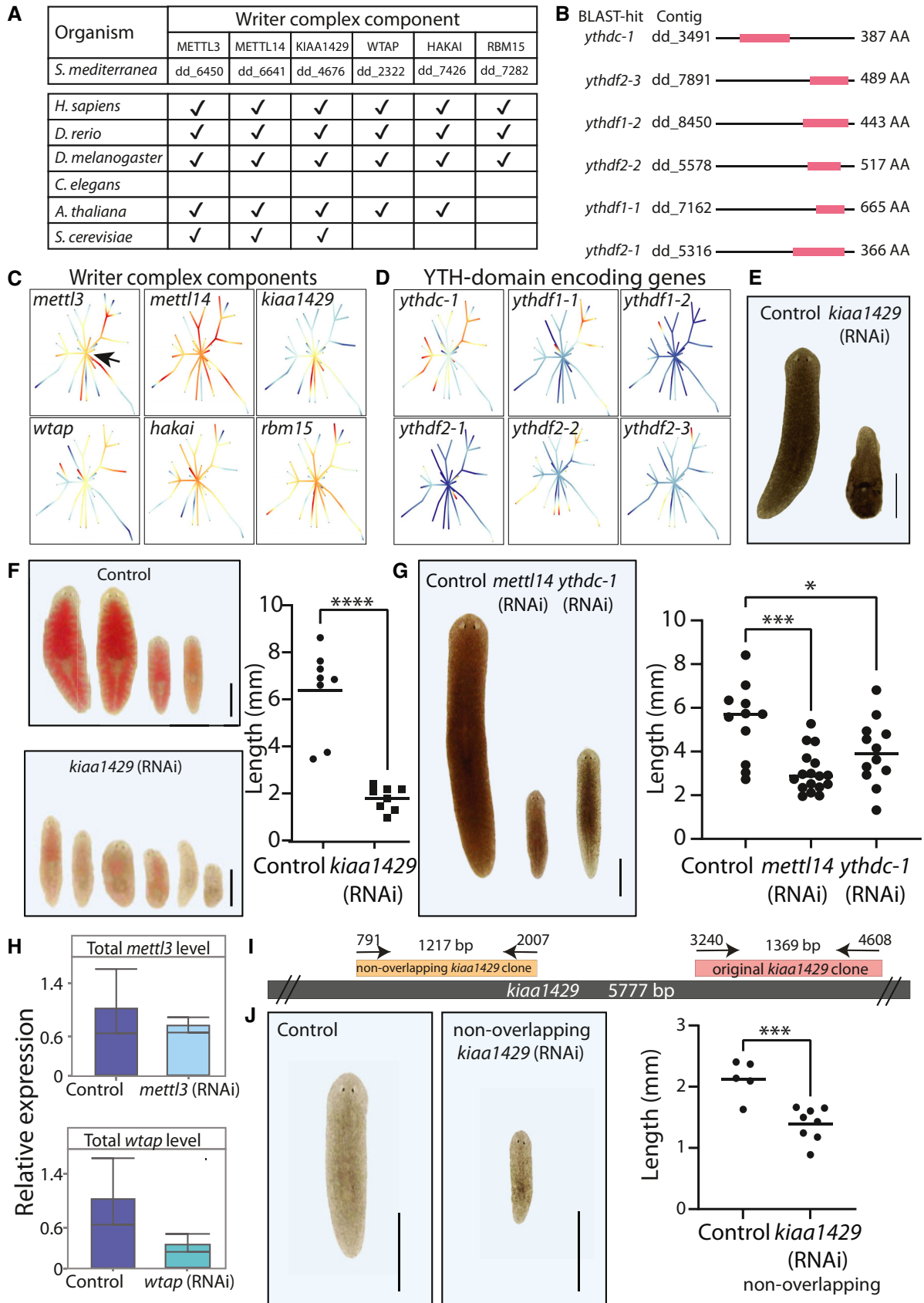


Figure EV1.

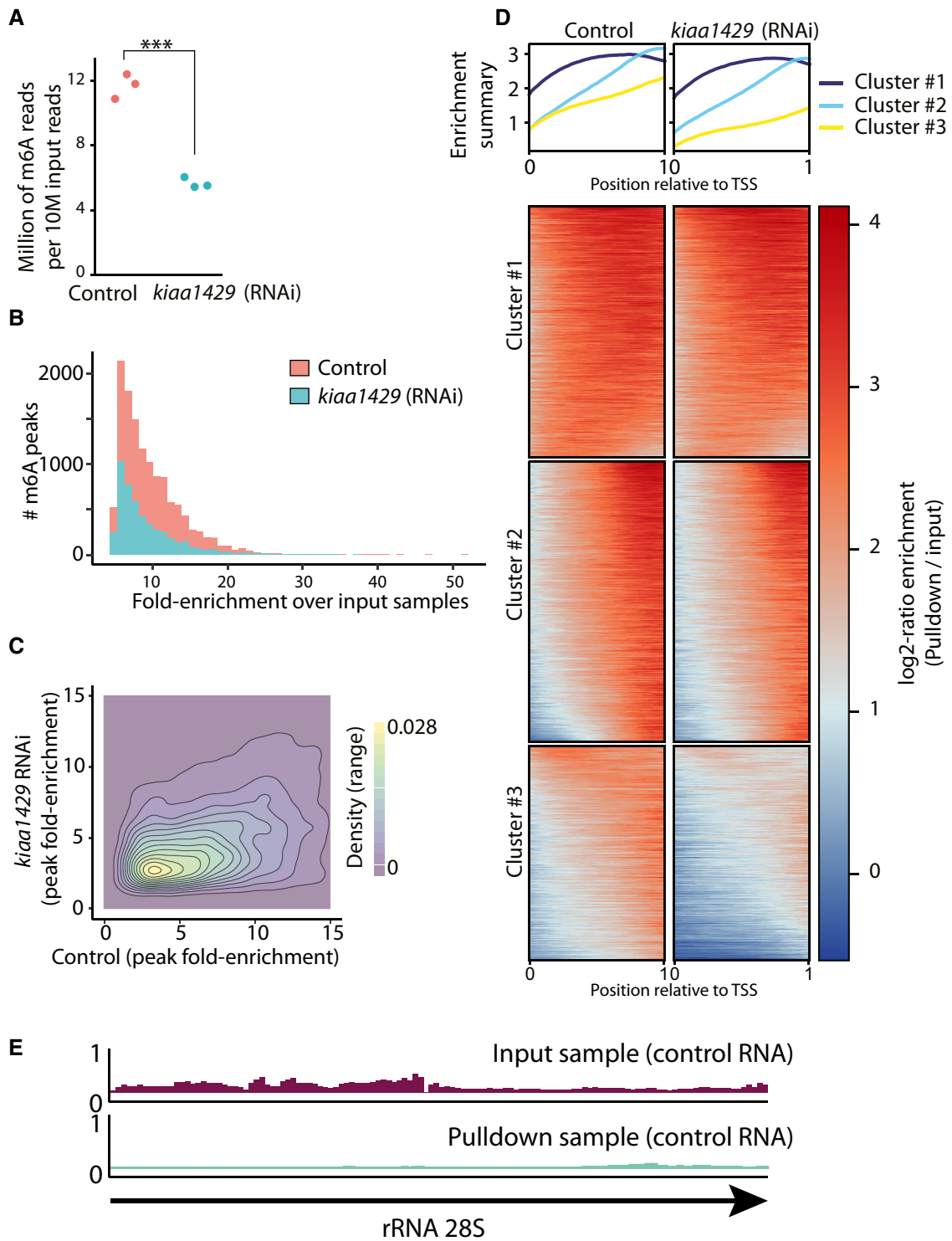
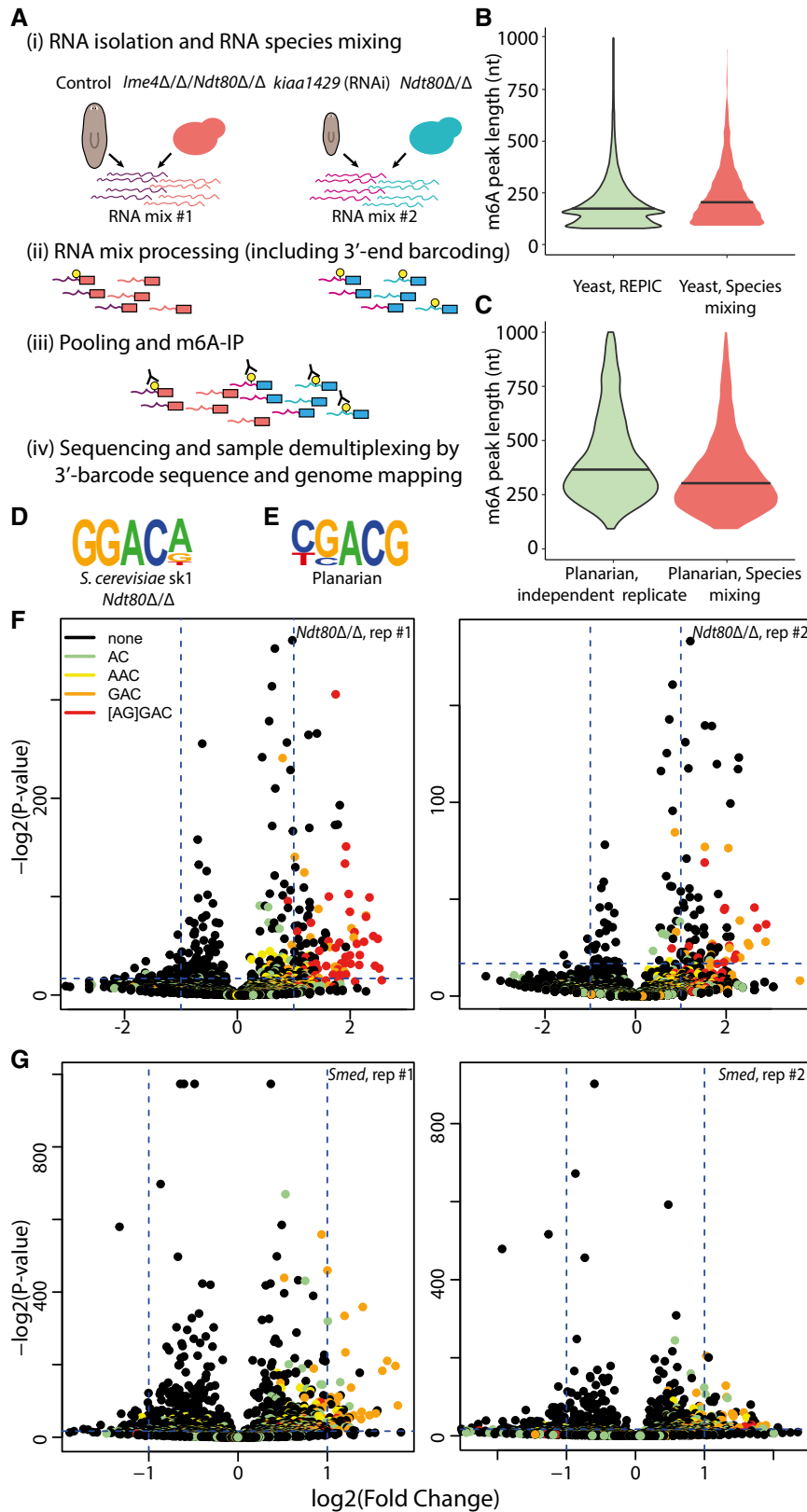


Figure EV2.

**Figure EV2. m6A is abundant on planarian mRNA and depleted following *kiaa1429* RNAi.**

- A The number of RNAseq reads for each m6A-seq2 pulldown library per 10 M of the corresponding input reads is shown. The number of reads in each pulldown library in the m6A-seq2 protocol correlates with the abundance of m6A (Dierks *et al*, 2021) (red and blue dot, control and *kiaa1429* (RNAi) sample, respectively). \*\*\*Student's *t*-test  $P < 0.001$ .
- B The number of m6A-rich regions (peaks) was larger in control samples and depleted following inhibition of *kiaa1429*. Moreover, the fold-enrichment of the peaks in the control samples over the gene expression observed in the input samples is greater, in comparison to the *kiaa1429* (RNAi) samples.
- C A 2d-density plot showing the correlation between m6A-enriched regions in control and *kiaa1429* (RNAi) animals. The density plot shows that m6a peaks were more highly enriched in the control samples compared to *kiaa1429* (RNAi) samples, demonstrating the depletion of m6A following inhibition of *kiaa1429*.
- D Profile of m6A-enriched regions across genes in control and *kiaa1429* (RNAi) showed enrichment toward the 3'-end. The length of transcripts with detectable m6A-enriched regions was normalized to 1,000 nt. Then, the expression across the transcript was computed by generating bins of gene expression (Materials and Methods) and calculating the log-fold change between the anti-m6A-antibody pulldown library and the input sample. K-means was used to separate three profiles of m6A-enriched regions.
- E Shown is the RPKM normalized expression of the planarian rRNA 28S (block arrow) in the m6A pulldown library and in control. There was no detectable m6A peak on planarian rRNA.



**Figure EV3. Analysis of m6A peak length by species mixing experiment.**

- A** RNA was extracted (i) from control or (ii) *kiaa1429* (RNAi) animals in duplicates, with at least 10 animals in each replicate, (iii) from meiosis-blocked *S. cerevisiae* strain with high levels of m6A (*Ndt80Δ/Δ*) (Dierks et al, 2021), and (iv) from *S. cerevisiae* strain devoid of m6A, due to deletion of the methyltransferase (*Ime4Δ/Δ/Ndt80Δ/Δ*). RNA was combined into two pools (Materials and Methods), and was processed according to the m6A-seq2 protocol (Dierks et al, 2021). Following sequencing, reads were associated with the original samples based on their 3'-end barcode (red and blue, representing mix #1 and mix #2, respectively), and then based on their mapping to either the planarian transcriptome or the yeast genome (Materials and Methods).
- B** Violin plot comparing the length of m6A peaks in yeast from either the REPIC database (Liu et al, 2020c), or from the data collected in this experiment; m6A regions larger than 1,000 bp were excluded from the plot, horizontal line indicates the median length.
- C** Comparison of planarian m6A peaks in our initial m6A-seq2 experiment, and in the m6A-seq2 profiling in the species RNA mixing experiment. Shown are peaks shorter than 1,000 bp. To avoid comparison of lowly enriched peaks, shown are peaks with fold-enrichments that are larger than the median fold-enrichment.
- D, E** Shown is the most frequent sequence motif detected in our mixed m6A-seq2 experiment (Materials and Methods), as detected by HOMER (Heinz et al, 2010) for yeast (D) and planarian (E).
- F, G** Shown are the fold change and associated P-values for each k-mer. DRACH-like k-mers are colored as in the figure legend. Data is shown for yeast (F; panels represent two biological replicates) and planarian (G; panels represent two biological replicates).

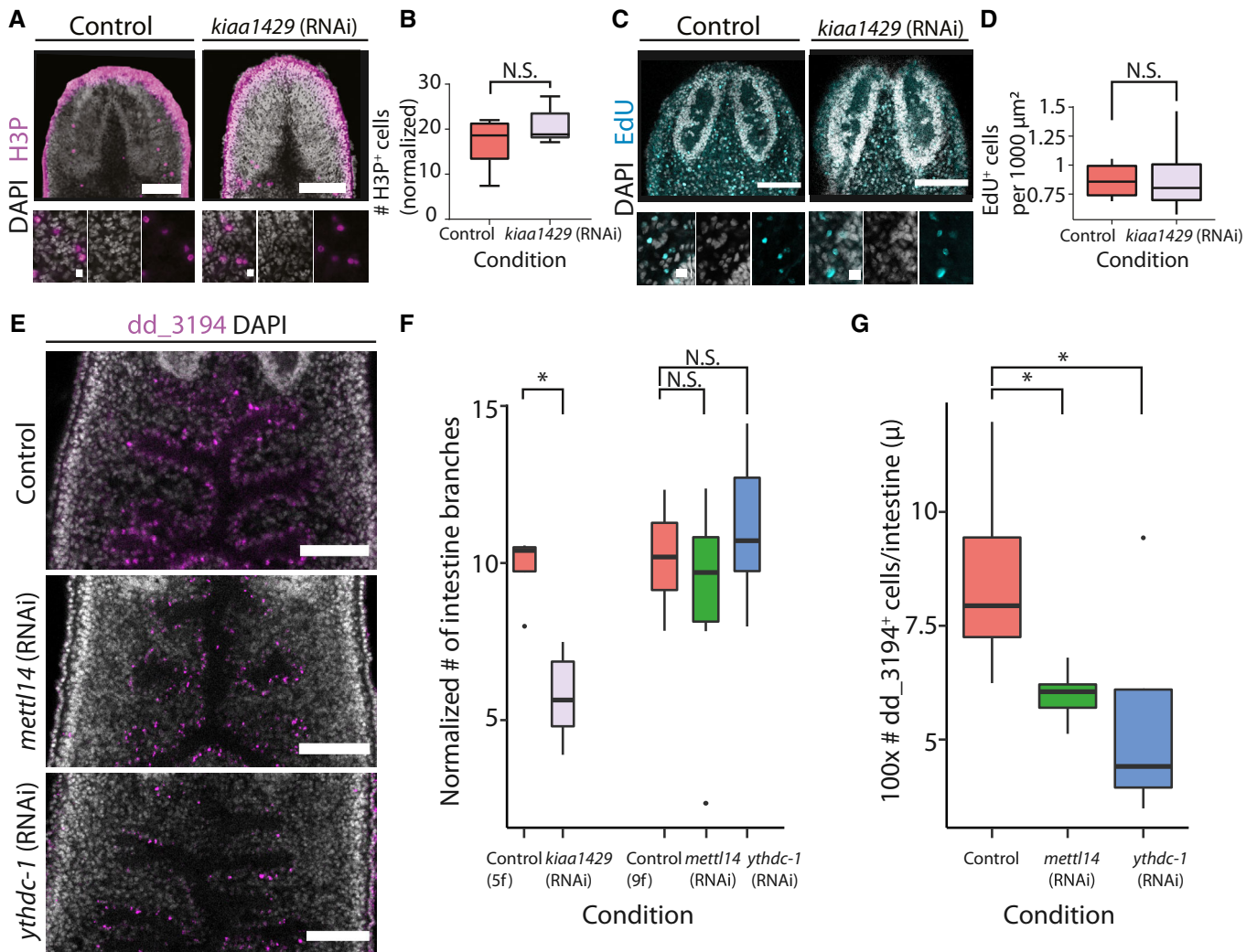


**Figure EV4. Reduction in intestinal cells following inhibition of m6A genes.**

A, B Shown is H3P labeling using an anti-H3P-antibody in *kiaa1429* (RNAi) and in control animals (scale = 100 and 10 μm, top and bottom panels, respectively; top panels show a maximal intensity projection of the H3P and DAPI signal; [Materials and Methods](#)). (B) The number of H3P<sup>+</sup> cells was counted in a region anterior to the pharynx and posterior to the brain, in a z-stack and was normalized to the area of the counting ([Materials and Methods](#)). There was an insignificant difference in the number of H3P<sup>+</sup> cells between the conditions (Student's *t*-test; *n* = 6 biological replicates). Boxes represent the IQR, whiskers represent the 1.5 × IQR, and central band represents the median.

C, D Shown are confocal images of *kiaa1429* (RNAi) and control animals, which were soaked in F-ara-EdU for 16 h (scale = 100 and 10 μm, top and bottom panels; [Materials and Methods](#)). (D) The number of F-ara-EdU<sup>+</sup> cells was counted in a region anterior of the pharynx and posterior to the brain and was normalized to the rectangle size ([Materials and Methods](#)). There was an insignificant difference in the number of F-ara-EdU<sup>+</sup> cells between the tested conditions (Student's *t*-test; *n* = 5 biological replicates). Boxes represent the IQR, whiskers represent the 1.5 × IQR, and central band represents the median.

E–G The effect of inhibition of m6A pathway-encoding genes on the intestine integrity and cells was examined by FISH. (E, F) Inhibition of *mettl14* (RNAi) or *ythdc-1* (RNAi) by 9 dsRNA feedings did not result in significant differences in the morphology of the intestine, as estimated by counting the number of intestine branches in confocal images ([Materials and Methods](#)). A significant difference in the number of intestine branches was observed following *kiaa1429* (RNAi) following five RNAi feedings compared to its control. Scale = 100 μm. (E, G) A significant reduction in the number of intestine cells labeled by dd\_3194 was found following either *mettl14* (RNAi) or *ythdc-1* (RNAi) (two-sided *t*-test controlled by Bonferroni's correction). The dd\_3194<sup>+</sup> cells were counted in confocal images and the counting was normalized to the length of the intestine branches ([Materials and Methods](#)). \**P* < 0.05.

**Figure EV5. Analysis of *kiaa1429* (RNAi) phenotypes by scRNAseq.**

- A–D Quality measurements of scRNAseq libraries prepared from control and *kiaa1429* (RNAi) cells. The quality of the libraries produced from both conditions was assessed using the Seurat package (Stuart *et al*, 2019). The number of expressed genes (A); unique molecular tags (B); non-coding gene expression (C); and the correlation between the number of expressed genes and the unique molecular tags were highly similar between the libraries (D). This indicated that the quality of libraries was comparable.
- E Expression levels of canonical neoblast markers were highly similar in control and *kiaa1429* (RNAi).
- F The polyadenylated transcript expression of *h2b* and *h3* was much higher in *kiaa1429* (RNAi) animals compared to controls. The expression was detectable in neoblasts (bottom), and to a much lesser degree in the entire cell population (top), which includes neoblasts as well.
- G, H UMAP representation of neoblasts (color dots, left panel), and their identity (right panel). Neoblast identity was assigned based on expression of previously published gene expression markers (Fincher *et al*, 2018). Most neoblast clusters were not affected by the RNAi, yet several lineages (right, asterisk) were differentially represented following *kiaa1429* (RNAi).
- I Expression of neoblast (*smedwi-1*) and specialized intestine neoblast gene expression markers was overlaid on UMAP plots of the intestine lineage (cells represented by dots; gray and purple, low to high ranked expression).
- J–L Comparison of gene expression between several cell clusters. Importantly, pharynx cells are post-mitotic, and therefore show minimal *smedwi-1* expression (J). Post-mitotic cells express *xbp-1*, which was previously shown to be expressed in differentiating and differentiated cells (Raz *et al*, 2021) (K). *SMAD6/7–2* is expressed in the *kiaa1429* (RNAi) specific-cluster and in neural cells (L).
- M Highly expressed genes in the *kiaa1429* (RNAi)-specific cluster compared to control are shown in UMAP plots. Contig dd\_1620 is highly expressed in the *kiaa1429* (RNAi)-specific cluster. The genes *SMAD6/7–2* and *protocadherin-like* (dd\_15376, gene model SMESG000067388) are expressed in the *kiaa1429* (RNAi)-specific cluster (black arrowhead); both genes are also expressed in cells of the neural clusters (e.g., cluster 2).

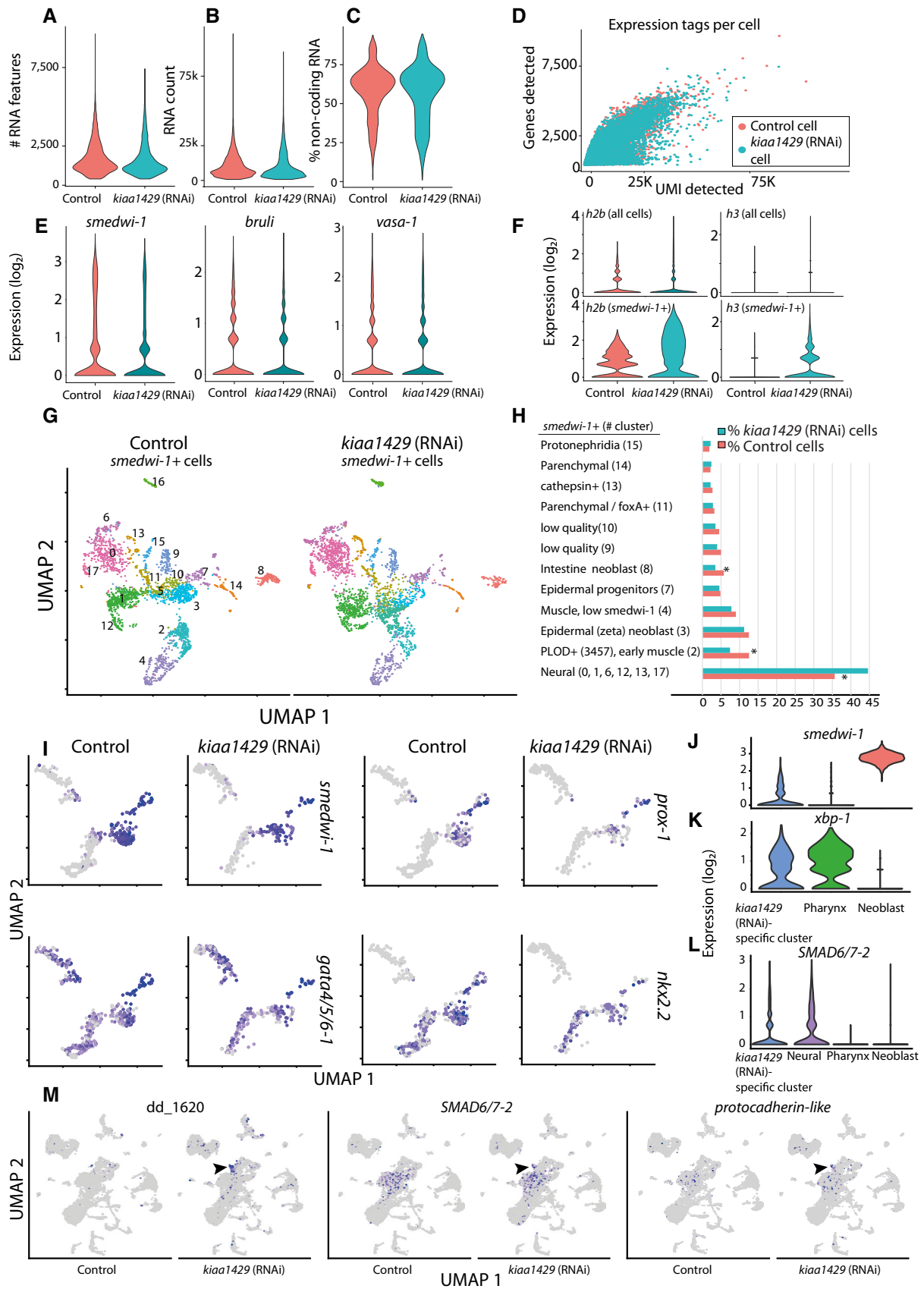


Figure EV5.

1 m6A is required for resolving progenitor identity during  
2 planarian stem cell differentiation

3 Yael Dagan<sup>1\*</sup>, Yarden Yesharim<sup>1\*</sup>, Ashley R. Bonneau<sup>2,3,4</sup>, Tamar Frankovits<sup>1</sup>, Schraga Schwartz<sup>5</sup>, Peter W.  
4 Reddien<sup>2,3,4</sup>, Omri Wurtzel<sup>1,6,7</sup>

5 <sup>1</sup> School of Neurobiology, Biochemistry, and Biophysics, The George S. Wise Faculty of Life Sciences, Tel Aviv University, 69978  
6 Tel Aviv, Israel

7 <sup>2</sup> Whitehead Institute for Biomedical Research, Cambridge, MA 02142, USA

8 <sup>3</sup> Department of Biology, Massachusetts Institute of Technology, Cambridge, MA 02139, USA

9 <sup>4</sup> Howard Hughes Medical Institute, Chevy Chase, MD 20815, USA

10 <sup>5</sup> Department of Molecular Genetics, Weizmann Institute of Science, 7610001 Rehovot, Israel

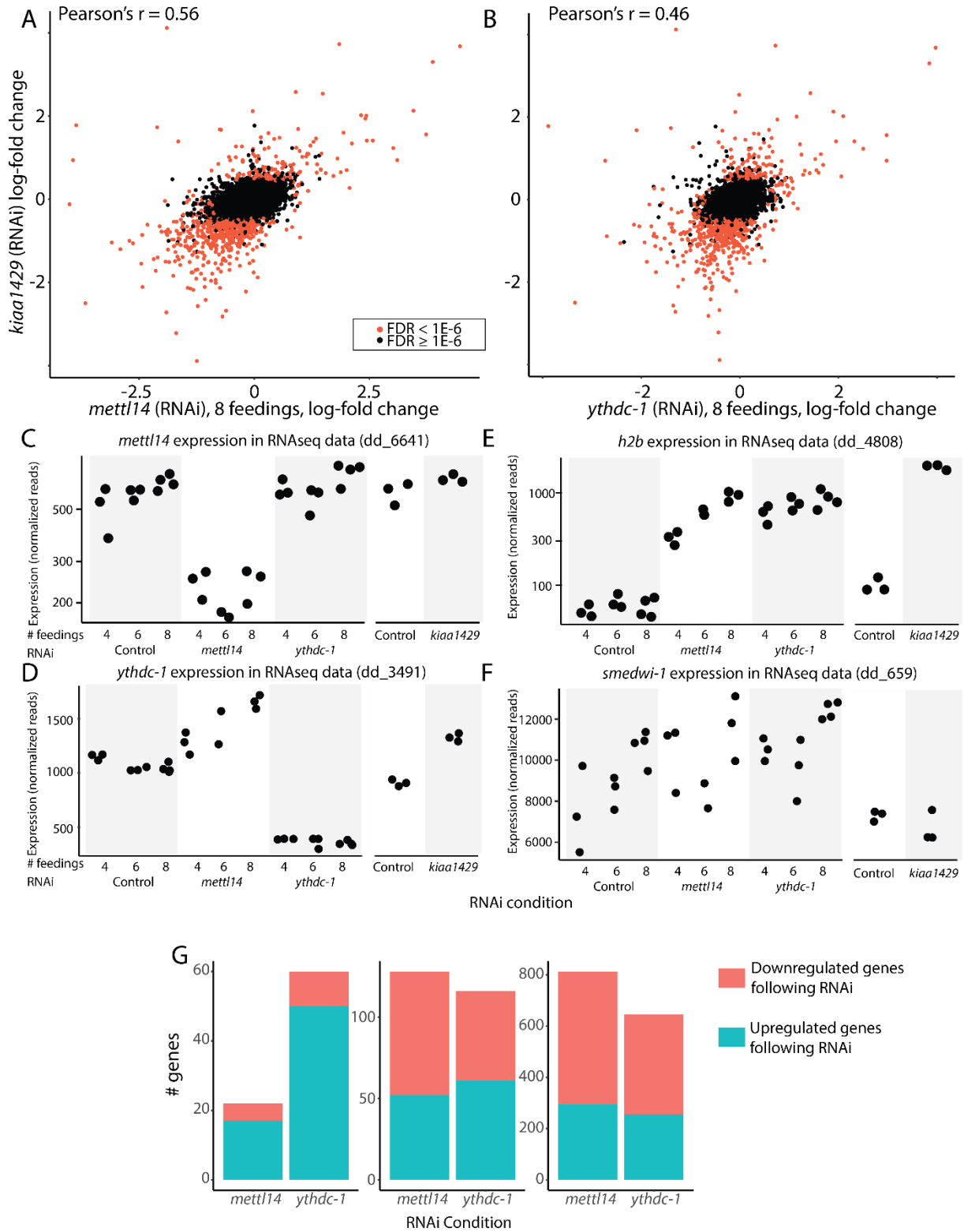
11 <sup>6</sup> Sagol School of Neuroscience, Tel Aviv University, Tel Aviv, Israel

12 \* These authors contributed equally

13 <sup>7</sup> Correspondence: owurtzel@tauex.tau.ac.il

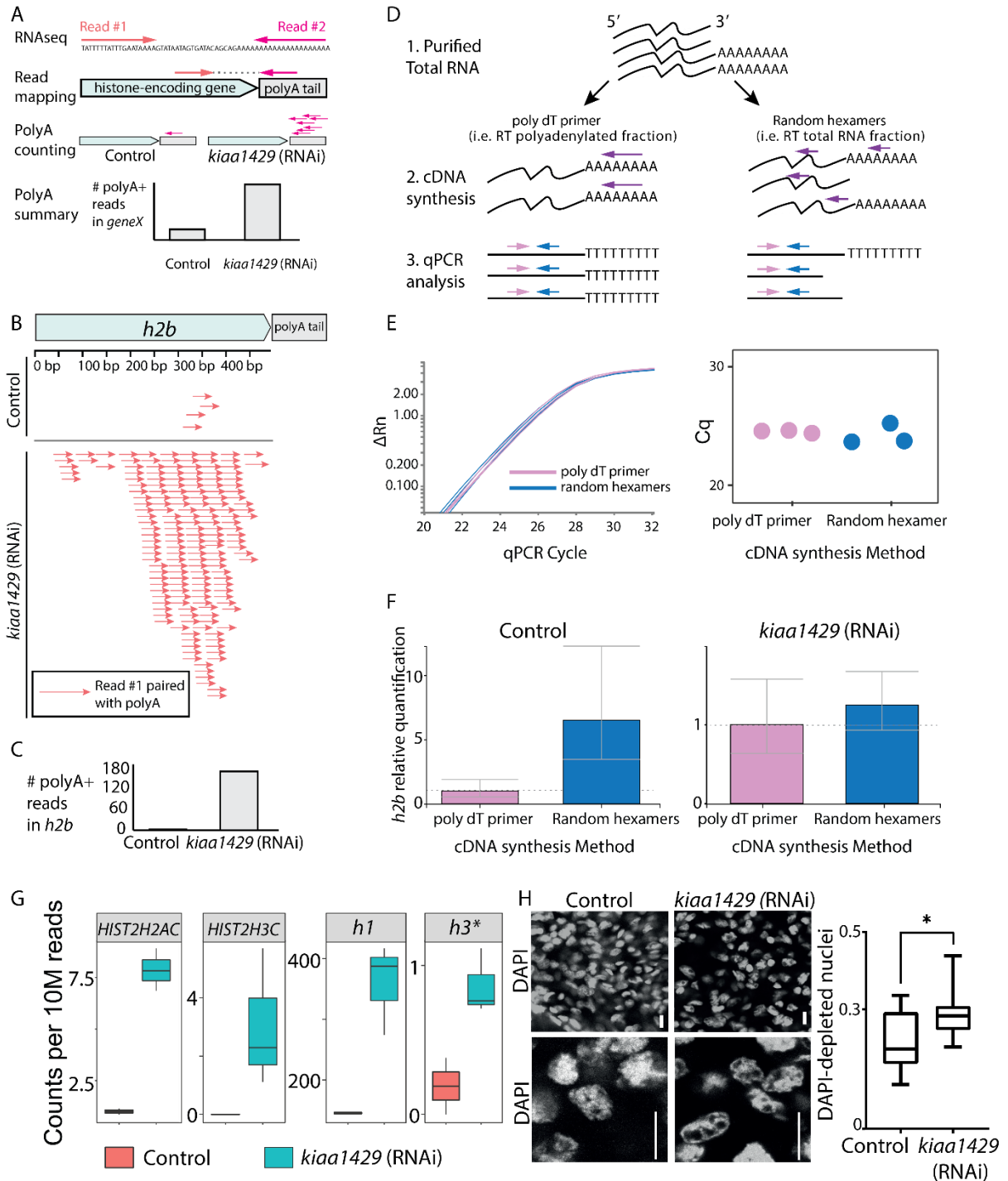
14	<b>Table of contents</b>	
15	Appendix Figure S1	3
16	Appendix Figure S2	5
17	Appendix Figure S3	7
18	Appendix Figure S4	8
19	Appendix Figure S5	10
20	Appendix Table S1. Gene models of contig IDs in figures	11
21	Appendix Table S2. Genes cloned in this study	12
22	Appendix Table S3. Inline m6A-seq2 barcode sequences	14
23	Appendix Table S4. Mapping of library data to the planarian transcriptome	15
24	Appendix Table S5. qPCR primers used in this study	17
25	Supplementary References	18
26		
27		

28 Appendix Figure S1



30 Appendix Figure S1. Specificity of RNAi of m6A genes. (A-B) Shown is the correlation in gene expression changes  
31 between experimental conditions. Each dot represents the log fold-change of a single gene, colored based on  
32 significance threshold (FDR threshold  $< 1E-6$ ). For both panels the p-value of the correlation  $< 2.2E-16$ . (C-F) Shown  
33 is the normalized gene expression in RPKM for genes across the different libraries. RNAseq analysis validated the  
34 efficiency and the specificity of the RNAi (C-D). The expression of *h2b* was upregulated in all of the tested  
35 conditions (E). By contrast, the expression of *smedwi-1* did not change significantly following inhibition of m6A  
36 genes (F). (E) The number of significantly upregulated and downregulated genes is shown at each of the tested  
37 time points (FDR of genes included  $< 1E-5$ ; Dataset EV2). In the early time point (four RNAi feedings) most of the  
38 genes were upregulated. However, at later time points, most differentially expressed genes are downregulated,  
39 which likely represent indirect effects of the RNAi, such as depletion of cell populations.

40 **Appendix Figure S2**

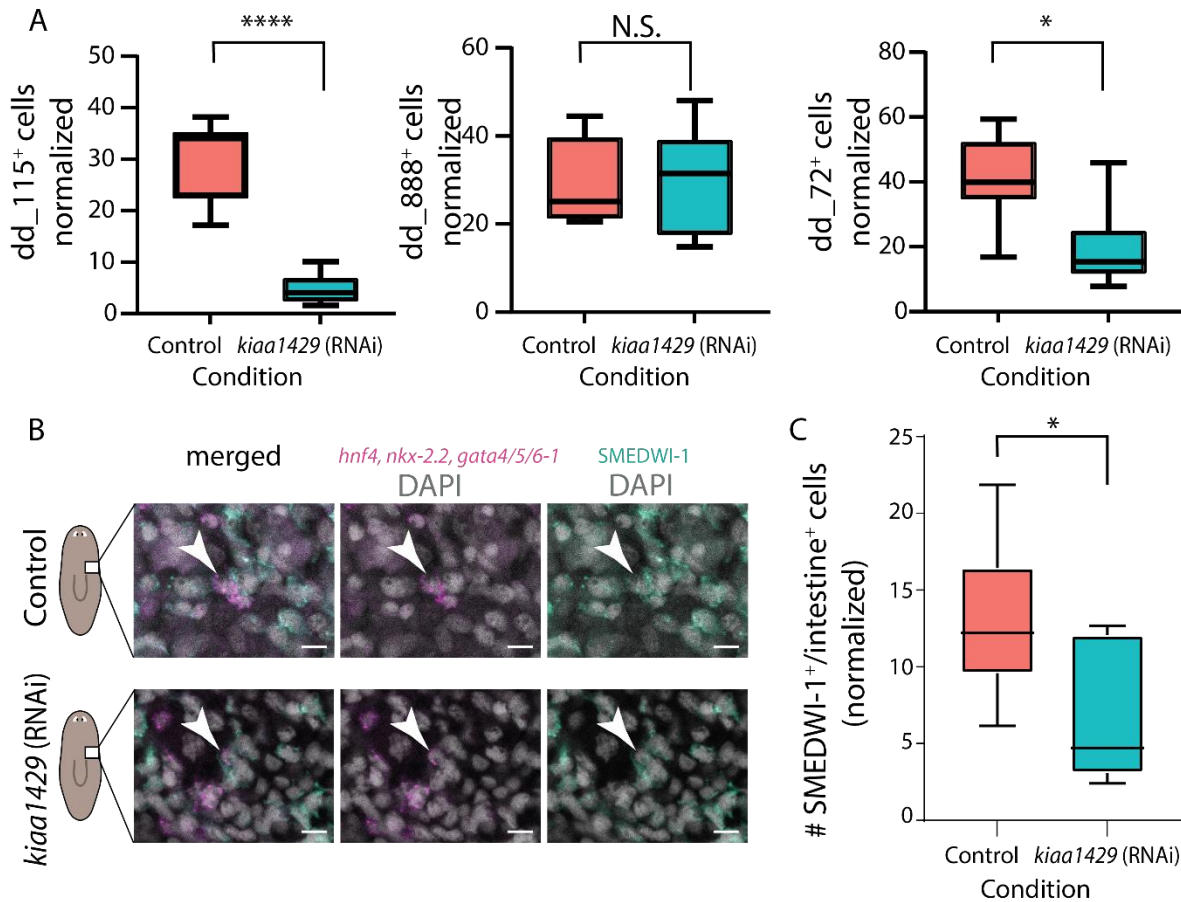


41

42 **Appendix Figure S2. Analysis of histone transcript polyadenylation following inhibition of m6A genes. (A) Paired-**  
 43 **end RNAseq data was used for identifying polyA containing histone transcripts. Reads mapped (read #1) to histone**

44 genes without proper read-pairing were computationally isolated, and their read pair (read #2) was collected from  
45 the raw data files. If the unmapped read (read #2) contained a poly-dT sequence, which is the reverse-complement  
46 of polyA, then the read was counted as a polyadenylated histone transcript. (B-C) Shown are RNAseq reads  
47 mapped to *h2b* (dd\_4808; gene model SMESG000067906), which had a paired-read (read #2) containing polyA.  
48 Control sample (top) has fewer reads mapped to *h2b* compared to the *kiaa1429* (RNAi) sample (bottom). The total  
49 number of polyA containing read-pairs mapped to *h2b* is shown in panel C. (D) qPCR strategy for estimating the  
50 fraction of polyadenylated and non-polyadenylated *h2b*. Purified RNA (1) was reverse-transcribed with a poly-dT,  
51 or random hexamers (2). Then, qPCR is performed with internal primers (3). (E) The expression of *gapdh* was  
52 measured using RNA that was purified from wild type planarians. The analysis was used to estimate the efficiency  
53 of qPCR using cDNA produced either with poly-dT priming or using random hexamers. The change in reporter  
54 signal (y-axis) as a function of the qPCR cycle was similar for both groups (left), as is the quantification cycle (C<sub>q</sub>,  
55 right). The analysis demonstrated that reverse-transcription with poly-dT and random hexamers was similarly  
56 efficient. (F) Shown in the relative quantification of polyadenylated *h2b* and non-polyadenylated *h2b* in control  
57 (left) and following *kiaa1429* (RNAi). The increase in polyadenylated *h2b* expression following *kiaa1429* (RNAi)  
58 was observed despite a lack of increase in total *h2b* expression (right). Error bars are the 95% confidence interval.  
59 (G) Shown is the number of polyA containing reads for several of the overexpressed histone components encoding  
60 genes in RNAseq data per 10M library reads (*h3\** is the putative *histone 3* transcript that is transcribed from contig  
61 dd\_25629, gene model SMESG000013634). Horizontal line indicates the median. (H) Comparison of DNA density  
62 by using DAPI-labeling on control and *kiaa1429* (RNAi) animals. DAPI-labeling, which correlates with chromatin  
63 density, showed an overabundance of DAPI-poor nuclei in *kiaa1429* (RNAi) animals. This suggested that *kiaa1429*  
64 (RNAi) chromatin packaging was altered, and indicated that euchromatin might be more prevalent in *kiaa1429*  
65 (RNAi), which might therefore affect transcriptional regulation. High magnification images (bottom) were  
66 acquired from different field-of-views from similar anatomical areas. Whiskers indicate the range of DAPI-poor-  
67 nuclei to nuclei ratio in the images, boxes indicate the interquartile range (IQR), and central band indicates the  
68 mean (n = 10 biological replicates per group). Student's t-test \* p < 0.05. Scale = 10 μm.

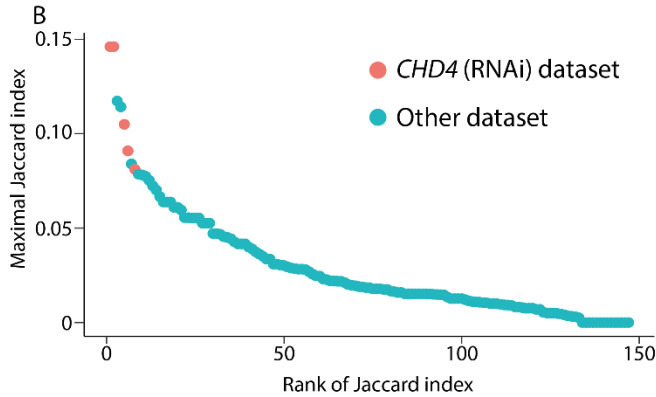
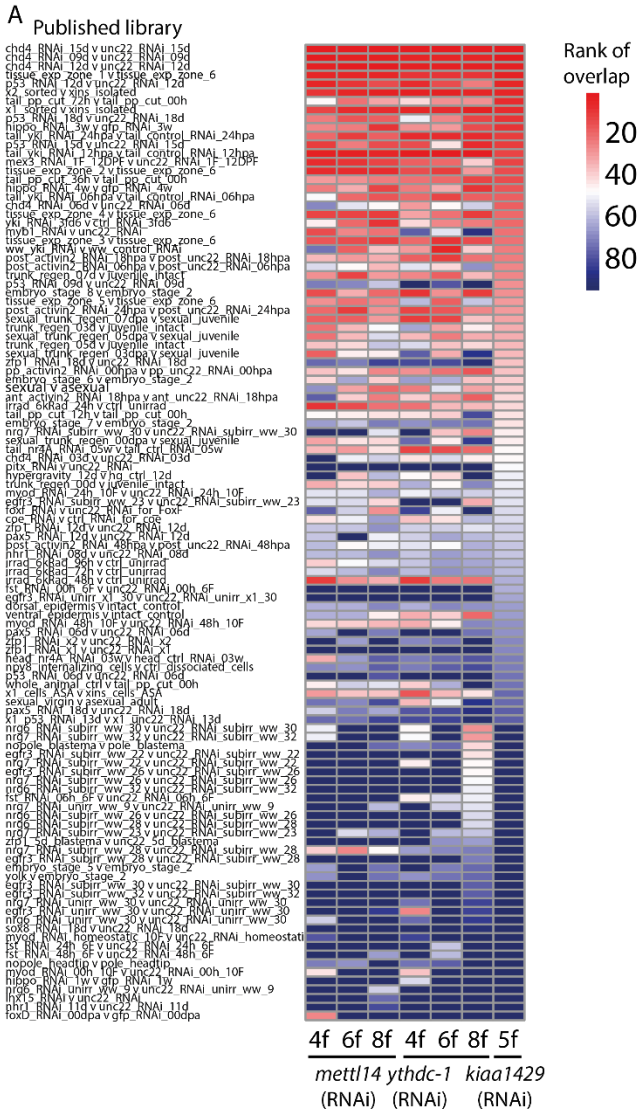
69 Appendix Figure S3



70

71 Appendix Figure S3. Reduction in intestinal cells following *kiaa1429* (RNAi). (A) Shown are cell counting of FISH  
 72 images in *kiaa1429* (RNAi) and in control animals normalized by the area of counting (rectangular region anterior  
 73 to the pharynx and posterior to the brain; Methods). Representative images are shown in Figure 6E (Two sided  
 74 Student's t-test  $p = 1.2E-7$  and  $0.001$  for dd\_115 and dd\_72, respectively followed by Bonferroni's correction). (B)  
 75 Shown is co-labeling of recently integrated intestinal cells into to intestine structure by using a mix probes for  
 76 detection of intestine-specific transcription factors (i.e., *hnf4*, *nkx-2.2*, and *gata4/5/6-1*), and anti-SMEDWI-1,  
 77 which labels neoblasts and recent progeny (Guo *et al*, 2006). White arrowheads indicate double positive cell. Scale  
 78 = 10  $\mu$ m. (C) Quantification of co-labeled SMEDWI-1+/intestine+ cells is shown in Control and *kiaa1429* (RNAi)  
 79 animals, based on cell counting from z-stack images (two sided Student's t-test = 0.02).

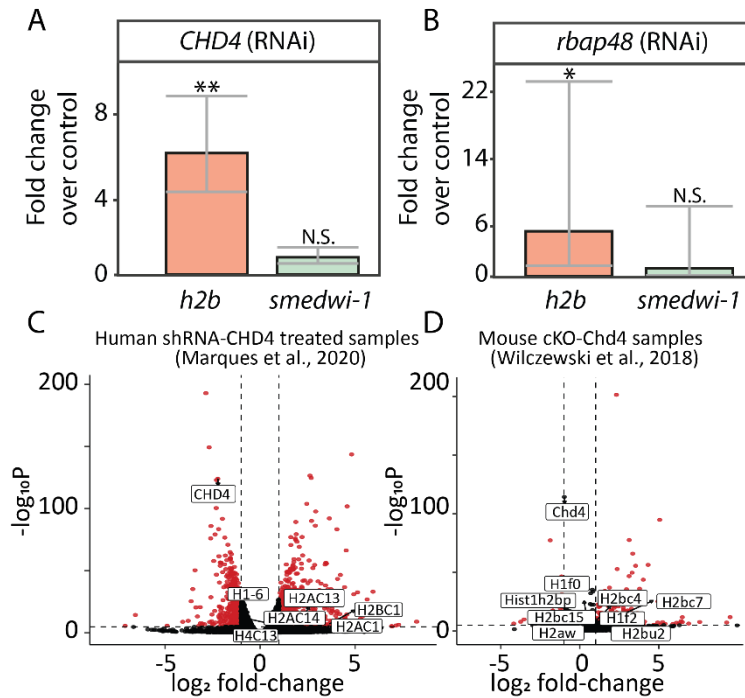
80 Appendix Figure S4



82 Appendix Figure S4. Overlap in differentially expressed genes. (A) Shown is the rank of overlap between the  
83 RNAseq libraries produced here and the published planarian datasets. The rank was determined by counting the  
84 number of overlapping and non-overlapping differentially expressed genes in the datasets produced here and in  
85 published datasets (FDR < 1E-5 and TPM > 10), and calculating the hypergeometric p-value for the overlap (Table  
86 EV1; blue to red, low and high ranked significance of overlap, respectively). (B) Plot showing the maximal Jaccard  
87 index calculated between up-to the top 200 differentially expressed genes in the published planarian datasets  
88 used here (Table EV1) and up-to the top 200 differentially expressed genes of each of the datasets produced here  
89 (Dataset EV2). Each dot represents a single dataset. *CHD4* (RNAi) datasets are highlighted in red.

90

91 **Appendix Figure S5**



92

93 **Appendix Figure S5. *CHD4* (RNAi) recapitulates molecularly the inhibition of m6A genes. (A-B) Shown is a qPCR**  
 94 **quantification of *h2b* and *smedwi-1* expression following RNAi of the NuRD component encoding genes *CHD4* (A)**  
 95 **or *rbap48* (B) in comparison to control libraries (error bars indicate the 95% confidence interval; two-sided t-test**  
 96 **Bonferroni corrected; \*\* -  $p < 0.01$ , \* -  $p < 0.05$ ). (C-D) volcano plot of human (C) and mouse (D) gene expression**  
 97 **changes following inhibition or conditional knockout of *CHD4* encoding gene (Marques *et al*, 2020; Wilczewski *et***  
 98 ***al*, 2018). Highlighted and labeled are significantly overexpressed histone-encoding genes, as well as the human**  
 99 **or mouse *CHD4* homolog (red and black, significant and non-significant change in gene expression; adjusted p-**  
 100 **value  $< 0.0001$ ).**

101 **Appendix Table S1. Gene models of contig IDs in figures**

Figure	Panel	Label in figure	Gene Model
Figure 2	A	dd_254	SMESG000073667
Figure 4	A	dd_783	SMESG000016810.1
Figure 4	A	dd_1837	SMESG000016779.1; SMESG000016781.1
Figure 4	A	dd_11930	SMESG000016771.1
Figure 4	A	dd_18852	SMESG000016780.1
Figure 4	A	dd_1616	SMESG000022742.1
Figure 4	A	dd_19404	NA
Figure 4	A	dd_15204	SMESG000081110.1
Figure 4	A	dd_20482	NA
Figure 4	A	dd_2089	SMESG000016811.1
Figure 4	A	dd_7261	NA
Figure 4	A	dd_2262	SMESG000038305.1
Figure 4	A	dd_1785	SMESG000005903.1; SMESG000006038.1
Figure 4	A	dd_1938	SMESG000007684.1
Figure 4	A	dd_4923	SMESG000063585.1
Figure 4	A	dd_6637	SMESG000071518.1
Figure 4	A	dd_2759	SMESG000081460.1
Figure 4	A	dd_3377	SMESG000026665.1
Figure 4	E	dd_175	SMESG000049722.1
Figure 4	E	dd_4575	SMESG000068883.1
Figure 4	E	dd_3194	SMESG000053627.1
Figure 5	A	dd_25629	SMESG000013634.1
Figure 5	H	dd_1837	SMESG000016779.1; SMESG000016781.1
Figure 5	H	dd_585	SMESG000062836.1
Figure 6	E	dd_72	NA
Figure 6	E	dd_888	SMESG000073691.1
Figure 6	E	dd_75	SMESG000027140.1
Figure 6	E	dd_115	SMESG000066413.1; SMESG000066416.1
Figure 7	E	dd_25269	SMESG000013634.1
Figure EV1	A	dd_6450	SMESG000034548.1
Figure EV1	A	dd_6641	SMESG000073528.1
Figure EV1	A	dd_4676	SMESG000074445.1; SMESG000074456.1; SMESG000074577.1; SMESG000074578.1
Figure EV1	A	dd_2322	SMESG000043489.1; SMESG000043668.1
Figure EV1	A	dd_7426	SMESG000019097.1
Figure EV1	A	dd_7282	SMESG000001341.1
Figure EV1	B	dd_3491	SMESG000018260.1
Figure EV1	B	dd_7891	SMESG000008619.1

Figure EV1	B	dd_8450	SMESG000003195.1
Figure EV1	B	dd_5578	SMESG000001953.1
Figure EV1	B	dd_7162	SMESG000039495.1
Figure EV1	B	dd_5316	SMESG000075874.1
Figure EV4	E	dd_3194	SMESG000053627.1
Figure EV4	G	dd_3194	SMESG000053627.1
Appendix Figure S1	A	dd_6641	SMESG000073528.1
Appendix Figure S1	B	dd_3491	SMESG000018260.1
Appendix Figure S1	C	dd_4808	SMESG000067906.1
Appendix Figure S1	D	dd_659	SMESG000036375.1
Appendix Figure S4	A	dd_115	SMESG000066413.1; SMESG000066416.1
Appendix Figure S5	A	dd_888	SMESG000073691.1
Appendix Figure S6	A	dd_72	NA

102 **Appendix Table S2. Genes cloned in this study**

Contig	Gene model	Primer ID	Sequence
dd_Smed_v4_4676_1	SMESG000074445	Kiaa1429_F	CCGCTATCCGTTGTTA TTATGCG
dd_Smed_v4_4676_1	SMESG000074445	Kiaa1429_R	TCCGTAATCGTGGCCAC GC
dd_Smed_v4_7282_1	SMESG000001341	rbm15_F	GGGAGTTATCTGATG GTCAAAGA
dd_Smed_v4_7282_1	SMESG000001341	rbm15_R	CCGGCACCCTAACA GAA
dd_Smed_v4_6450_0_1	SMESG000034548	mettl3_F	AATTGAAACCAGACG AAATGCA
dd_Smed_v4_6450_0_1	SMESG000034548	mettl3_R	AGGTGTGTGGTTGCA GAGG
dd_Smed_v4_7426_1	SMESG000019097	hakai_F	ACGGTCAATGTCTCGT AGCC
dd_Smed_v4_7426_1	SMESG000019097	hakai_R	GCACGGCATCATGTTT AGG
dd_Smed_v6_2322_4	SMESG000043489	wtap_F	CCCGATGAAATGGTG AAATC
dd_Smed_v6_2322_4	SMESG000043489	wtap_R	TCGGGATCATCCTCTT CATC

dd_Smed_v4_3491_0_1	SMESG000018260	ythdc-1_F	CAGTCATCTCCCAATG TTGACG
dd_Smed_v4_3491_0_1	SMESG000018260	ythdc-1_R	ACAAACCGCAATAATT GTAACCA
dd_Smed_v6_3194_0_1	SMESG000053627	Intestine marker_F	GATCGAGGAAATCTT GACGAAC
dd_Smed_v6_3194_0_1	SMESG000053627	Intestine marker_R	GTGAATACTTCAGGA GCCATCC
dd_Smed_v6_175_0_1	SMESG000049722	<i>cathepsin+</i> marker_F	ACGATCTCGGAAAAC ATTTCG
dd_Smed_v6_175_0_1	SMESG000049722	<i>cathepsin+</i> marker_R	AGCCATCGTAGCTATT CCACA
dd_Smed_v6_701_0_1	SMESG000077782	collagen F	GTGGAGAAGCTTGGAG CAAGC
dd_Smed_v6_701_0_1	SMESG000077782	collagen R	AACACCAGCATCTCCT GGAC
dd_Smed_v6_4575_0_1	SMESG000068883	Protonephridia_F	CAACCCCAACGCGATA CAAT
dd_Smed_v6_4575_0_1	SMESG000068883	Protonephridia_R	CAGAAAGAAAGAGCC TCCGC
dd_Smed_v4_4676_1	SMESG000074445	<i>kiaa1429</i> non-overlapping_F	AGGACGTTTCCAGCAA TGAG
dd_Smed_v4_4676_1	SMESG000074445	<i>kiaa1429</i> non-overlapping_R	CATGGTTCGCCTTGGGA TTAG
dd_Smed_v6_2331_0_1	SMESG000068192	<i>CHD4</i> _F	CGCGAGCATTTTCATCT TGTA
dd_Smed_v6_2331_0_1	SMESG000068192	<i>CHD4</i> _R	AAACGATGGGCTTCAT CAAC
dd_Smed_v6_2065_0_1	NA	<i>rbAp48</i> _F	GAATGGCCAAGCTTA ACTGC
dd_Smed_v6_2065_0_1	NA	<i>rbAp48</i> _R	TTTGGGCTCCAAGCTGA AATC
dd_Smed_v6_115_0_1	SMESG000066413	Intestine marker_F	CAGTGCTTGCCGTCTG TCTA

dd_Smed_v6_115_0_1	SMESG000066413	Intestine marker_R	TAGCAACCAGTGCATT GAGC
dd_Smed_v4_72_0_1	NA	Intestine marker_F	AATGTTGGGATGCTGC AGTT
dd_Smed_v4_72_0_1	NA	Intestine marker_R	CAAAACGCAGGGCTC ATACT
dd_Smed_v4_75_0_1	SMESG000027140	Intestine marker_F	TGCCGTTATGAACATG ATTTTCG
dd_Smed_v4_75_0_1	SMESG000027140	Intestine marker_R	ACACAAAATATCGCAT CCTGCC
dd_Smed_v4_888_0_1	SMESG000073691	Intestine marker_F	TCTTGGACTTCATCGA CTTTCT
dd_Smed_v4_888_0_1	SMESG000073691	Intestine marker_R	AACTGGTTTTTCGTTGT CTACAAA
dd_Smed_v6_1837_0_1	SMESG000016779	<i>kiaa1429</i> -cluster #1 F	TTGGAACAGACCACTG GTGA
dd_Smed_v6_1837_0_1	SMESG000016779	<i>kiaa1429</i> -cluster #1 R	AACGACGACCTTTCCA ACTG
dd_Smed_v6_585_0_1	SMESG000062836	<i>kiaa1429</i> -cluster #2 F	ACAAGTGCAATGCC GTAAC
dd_Smed_v6_585_0_1	SMESG000062836	<i>kiaa1429</i> -cluster #2 R	CCTCATTTCCACGGT ATCA

103 **Appendix Table S3. Inline m6A-seq2 barcode sequences**

Condition	Replicate	Barcode sequence	Experiment
<i>kiaa1429</i> (RNAi)	#1	NNNCCAGTCT	m6A-seq2
<i>kiaa1429</i> (RNAi)	#2	NNNCCTCCGT	m6A-seq2
<i>kiaa1429</i> (RNAi)	#3	NNNGCACTCT	m6A-seq2
<i>unc22</i> (RNAi), Control	#1	NNNGCCCATT	m6A-seq2
<i>unc22</i> (RNAi), Control	#2	NNNGGCCTCT	m6A-seq2
<i>unc22</i> (RNAi), Control	#3	NNNTATCACT	m6A-seq2

<i>unc22</i> (RNAi), Control <i>lme4Δ/Δ/Ndt80Δ/Δ</i>	#1	NNNGTTTGCT	Species mixing m6A-seq2
<i>unc22</i> (RNAi), Control <i>lme4Δ/Δ/Ndt80Δ/Δ</i>	#2	NNNCCTTAGT	Species mixing m6A-seq2
<i>kiaa1429</i> (RNAi) <i>Ndt80Δ/Δ</i>	#1	NNNCAACTGT	Species mixing m6A-seq2
<i>kiaa1429</i> (RNAi) <i>Ndt80Δ/Δ</i>	#2	NNNCACCTCT	Species mixing m6A-seq2

104 **Appendix Table S4. Mapping of library data to the planarian transcriptome**

Condition	Type	Mapping ratio	Unmapped read ratio
<i>kiaa1429</i> (RNAi)	Input	0.871783	0.128217
<i>kiaa1429</i> (RNAi)	pulldown	0.876082	0.123918
<i>kiaa1429</i> (RNAi)	Input	0.872294	0.127706
<i>kiaa1429</i> (RNAi)	pulldown	0.88221	0.11779
<i>kiaa1429</i> (RNAi)	Input	0.88312	0.11688
<i>kiaa1429</i> (RNAi)	pulldown	0.885548	0.114452
Control	Input	0.886476	0.113524
Control	pulldown	0.895546	0.104454
Control	Input	0.840594	0.159406
Control	pulldown	0.891526	0.108474
Control	Input	0.882362	0.117638

Control	pulldown	0.893802	0.106198
---------	----------	----------	----------

105

106 **Appendix Table S5. qPCR primers used in this study**

<b>Gene</b>	<b>Sequence</b>	<b>Contig</b>	<b>Gene model</b>
<i>11930_F</i>	GAGGATTCTCCTATTAACCC AAC	dd_smed_v6_11930 _0_1	SMESG00001 6771
<i>11930_R</i>	CGTGCGATCAGCGTTTATATT	dd_smed_v6_11930 _0_1	SMESG00001 6771
<i>gapdh_F*</i>	TCTTCCCAACCAATTTTCTGT TCTG	dd_smed_v6_78_0_ 1	SMESG00005 2353
<i>gapdh_R*</i>	CCGAATATTTTATTTGGCTCTT CCTCCA	dd_smed_v6_78_0_ 1	SMESG00005 2353
<i>smedwi1_F*</i>	GTCTCAGAAAACAATAAAGG TACAGCA	dd_smed_v6_659_0 _1	SMESG00003 6375
<i>smedwi1_R*</i>	TGCTGCAATACACTCGGAGAC A	dd_smed_v6_659_0 _1	SMESG00003 6375
<i>mettl3_F</i>	ACAGTTTTGTCCTATGGTAC C	dd_Smed_v6_6450_ 0_1	SMESG000034 548
<i>mettl3_R</i>	GAAAGCAAGTATTGAGAAAT GAAC	dd_Smed_v6_6450_ 0_1	SMESG000034 548
<i>wtap_F</i>	GGAGCTGATTTCCATTAAGAA TG	dd_Smed_v6_2322_ 0_4	SMESG000043 489
<i>wtap_R</i>	TCGATATTGATTTTGCACACT G	dd_Smed_v6_2322_ 0_4	SMESG000043 489
<i>3194_F</i>	CATTTGTGCTATTACGGTGTC	dd_smed_v6_3194_ 0_1	SMESG000053 627
<i>3194_R</i>	GGTGAGTTCATTAGTGACAG	dd_smed_v6_3194_ 0_1	SMESG000053

	C	0_1	627
<i>h2b_F</i>	TGTAAGGTTGATTTTACCAGG AG	dd_smed_v6_4808_ 0_1	SMESG00006 7906
<i>h2b_R</i>	CCCGTGTACTTAGTAACAGC	dd_smed_v6_4808_ 0_1	SMESG00006 7906
<i>rbm15_F</i>	GGCGAATTCAATGTCAAAGTA G	dd_Smed_v6_7282_ 0_1	SMESG00000 1341
<i>rbm15_R</i>	AGCCAAAACAGGATCAACTG	dd_Smed_v6_7282_ 0_1	SMESG00000 1341

107 \* Primer sequences previously published (van Wolfswinkel *et al*, 2014).

## 108 **Supplementary References**

109 Guo T, Peters AHFM & Newmark PA (2006) A *bruno-like* gene is required for stem cell  
110 maintenance in planarians. *Dev Cell* 11: 159–169

111 Marques JG, Gryder BE, Pavlovic B, Chung Y, Ngo QA, Frommelt F, Gstaiger M, Song Y,  
112 Benischke K, Laubscher D, *et al* (2020) NuRD subunit CHD4 regulates super-enhancer  
113 accessibility in rhabdomyosarcoma and represents a general tumor dependency. *eLife* 9

114 Wilczewski CM, Hepperla AJ, Shimbo T, Wasson L, Robbe ZL, Davis IJ, Wade PA & Conlon FL  
115 (2018) CHD4 and the NuRD complex directly control cardiac sarcomere formation. *Proc Natl*  
116 *Acad Sci USA* 115: 6727–6732

117 van Wolfswinkel JC, Wagner DE & Reddien PW (2014) Single-cell analysis reveals functionally  
118 distinct classes within the planarian stem cell compartment. *Cell Stem Cell* 15: 326–339